Decadal Thermocline Variability in the North Pacific Ocean: Two Pathways around the Subtropical Gyre

RONG-HUA ZHANG

Graduate School of Oceanography, University of Rhode Island, Narragansett, Rhode Island

ZHENGYU LIU

Department of Atmospheric and Oceanic Sciences, University of Wisconsin—Madison, Madison, Wisconsin

(Manuscript received 20 September 1997, in final form 7 December 1998)

ABSTRACT

Yearly in situ temperature anomaly data in the North Pacific Ocean for 1961–90 have been analyzed along constant-density surfaces (isopycnals) in order to better describe and understand decadal thermocline variability in the region. Various empirical orthogonal function analyses are performed on isopycnals to depict the dominant three-dimensional patterns. The major finding is of two preferential pathways associated with decadal temperature variability around the subtropical gyre. A subduction pathway, with a large signal in the upper thermocline, originates from the North Pacific central–eastern outcrop regions (about 40°N, 150°W) and then basically follows the mean gyre circulation southwestward along isopycnals toward the western Tropics. A subtropical pathway extends from the eastern subtropical–tropical and boundary regions and appears to continue predominantly westward across the southern part of the gyre (between 15° and 30°N) and then along the Kuroshio path toward the midlatitudes. Along these two pathways, thermal anomalies show coherent phase relationships to one another in the surface layer and in the thermocline around the gyre, with their source regions (variability centers) being out of phase on decadal timescales. Two examples of each type of anomaly pattern can be illustrated for the periods analyzed. In the 1960s, a negative temperature anomaly signal propagated predominantly westward across the subtropics, followed by a subducted warm anomaly from the outcrop region in the early 1970s that subsequently moved southwestward along isopycnals toward the western Tropics. A similar pattern was observed in the late 1970s and in the 1980s but with the opposite sign: a westward propagating positive temperature anomaly signal along the subtropics in the late 1970s through the 1980s, and a subducted cold anomaly in the early 1980s that also made its way southwestward with the expected gyre circulation to the western Tropics in the late 1980s. It is suggested that the southwestward subduction pathway provides a mechanism that connects surface anomalies in the outcrop region to thermocline variations in the western subtropics and in the Tropics, and that the westward subtropical pathway presents a possible link of tropical–subtropical variability to surface temperature anomalies around the Kuroshio and its extension regions, which may further force variations in the overlying atmospheric circulation in the midlatitudes. The results provide an observational basis for verification of theoretical studies and model simulations.

1. Introduction

There is increasing observational evidence that the ocean thermocline in the North Pacific undergoes significant decadal changes (e.g., Levitus et al. 1994b; Levitus and Antonov 1995; Deser et al. 1996; White and Cayan 1998; and others). Consistent with the identification of different dynamical regimes from theoretical predictions of the ventilated thermocline models (Luyten et al. 1983; Huang and Russell 1994), decadal ocean variability can be strikingly different around the subtropical gyre (Liu 1993; Liu and Pedlosky 1994; Liu 1996). Clearly, different processes may be responsible for initiating and maintaining these decadal anomalies, such as the Rossby wave mechanism (e.g., Latif and Barnett 1994, 1996; Jacobs et al. 1994; Jin 1997) and the subduction mechanism (e.g., Deser et al. 1996; Gu and Philander 1997; Zhang et al. 1998; Liu 1999a,b; Huang and Pedlosky 1999; Schneider et al. 1999).

Zhang and Levitus (1997) presented an observational description of the three-dimensional structure and time evolution of decadal upper-ocean temperature variability in the North Pacific. One dominant pattern is characterized by a clockwise rotation of subsurface temperature anomalies around the subtropical gyre, closely following the mean circulation. This signal appears to be associated with the subduction of temperature anom-

Corresponding author address: Rong-Hua Zhang, International Research Institute for Climate Prediction, Lamont-Doherty Earth Observatory, Columbia University, 61 Route 9W, Palisades, NY 10964. E-mail: rzhang@iri.ldeo.columbia.edu

alies in the midlatitude outcrop region as first identified by Deser et al. (1996). Another pattern features a westward trans-Pacific propagating signal that is most pronounced and significant in the subtropics. This partially reflects a Rossby wave motion (e.g., Jacobs et al. 1994; Chelton and Schlax 1996). These two signals are still evident in decadal temperature variations even at 400-m depth (Zhang 1998). More recently, Miller et al. (1998) and Deser et al. (1999) provided evidence for a westward intensified signal associated with decadal temperature variability at 400-m depth in the midlatitudes.

At present, there is limited understanding of decadal thermocline variability around the North Pacific subtropical gyre. Its origin is not clear and its role in the Pacific decadal climate changes is in debate (Trenberth and Hurrel 1994; Graham 1994; Miller et al. 1994; Latif and Barnett 1994, 1996). Some important questions remain to be further investigated. What processes contribute to the initiation and maintenance of thermocline anomalies on decadal timescales? What are possible preferential pathways of decadal thermocline anomalies around the North Pacific subtropical gyre? To what extent can the observed patterns be understood according to recently developed thermocline theories (e.g., Liu 1999a,b; Huang and Pedlosky 1999)?

In this paper, we analyze observed upper-ocean temperature anomaly fields (Levitus et al. 1994b) to investigate decadal, three-dimensional thermocline variability in the North Pacific. Different from previous analysis done mostly at constant-depth levels, the present analysis is performed on constant-density surfaces (isopycnals) whose horizontally varying depths are estimated from long-term mean climatology. In addition, some dynamical quantities defining water pathways are evaluated on isopycnals, which help explain physically the decadal anomaly patterns around the subtropical gyre. Since thermocline anomalies tend to move along isopycnal surfaces in the extratropics (e.g., Deser et al. 1996; Zhang et al. 1998), an isopycnal analysis can present three-dimensional structure and time evolution in a natural and a physical way. Indeed, the sloping of isopycnal surfaces with depth is not uniform in the horizontal. In the subtropics, isopycnal surfaces are found at greater depths; with increasing latitude they rise and eventually intersect the sea surface in the midlatitudes (outcropping). The outcrop regions provide windows through which surface mixed layer water can enter the thermocline; the subducted water then most likely moves along isopycnal surfaces, suggesting that an isopycnal analysis could enable us to trace its pathways coherently throughout the gyre. This may provide a better opportunity for describing and understanding the link between temperature anomalies in the thermocline and at the sea surface across the subtropical gyre-scale regimes.

A brief description of data sources and analysis procedures is given in section 2, followed in section 3 by a description of mean flow patterns and the standard deviation of temperature anomalies evaluated on isopycnals. In section 4, we examine decadal thermocline variability on isopycnals to illustrate two dominant pathways around the subtropical gyre. This is further demonstrated in section 5 by using results of EOF analyses. Finally, section 6 gives conclusions.

2. Upper-ocean temperature data and isopycnal analyses

The data used in this study were the yearly in situ temperature anomaly fields at constant-depth levels given by Levitus et al. (1994b). These fields represent objective analyses of historical temperature profiles available at the National Oceanic and Atmospheric Administration/National Oceanographic Data Center (NOAA/NODC) through December 1993. These observational profiles have been analyzed in a consistent, objective manner on a 1° lat–long grid at standard oceanographic analysis levels between the sea surface and a depth of 400 m. Data sources, quality control, and analysis procedures were described in detail by Levitus and Boyer (1994).

Since we are interested in describing decadal, basinwide anomaly patterns, we further prepared datasets on a 5° lat–long grid by averaging the temperature anomalies from the 1° lat–long grid values. The grid points produced are centered at 2.5°, 7.5°, 12.5°N, etc., latitude, and at 122.5°, 127.5°, 132.5°E, etc., longitude, respectively. Within the limitation of observed data (nonsynoptic, scattered in space), the coarse resolution chosen can include more data observations in the 5° × 5° grid box than in the original 1° × 1° grid box, thus giving a more reliable estimate of observed temperature anomalies. Another reason for choosing the coarse resolution is the computation limitation in performing a combined EOF analysis (see section 5) on temperature anomaly data of entire upper-ocean layers. Our previous analyses (Zhang and Levitus 1997) indicate that this coarse resolution appears to be appropriate to describe decadal patterns in the North Pacific. To produce yearly anomaly fields, 30-yr averaged values during 1961–90 were subtracted from those for each individual year. Then a 3-yr running mean was performed to highlight decadal-scale signals.

Finally, we obtain temperature anomalies on constant-density surfaces using the following simple procedure. First, mean depth of an isopycnal surface is estimated from in situ density fields that are calculated from annual mean temperature and salinity data (Levitus and Boyer 1994; Levitus et al. 1994a). Then, at every horizontal grid, temperature anomalies at constant-depth levels are vertically interpolated onto the depth of the isopycnal surface by using a cubic spline. In this way, we do not take into account variations in the mean structure of density because of the lack of basinwide, varying salinity observations. This procedure would be reasonable for describing large-scale decadal variability in the region of interest. Since observed temperature anomalies

in the extratropical thermocline are small on decadal scales (e.g., the amplitude is generally less than 0.6°C away from the eastern boundary region) and their effect on density can be compensated for by correlated changes in salinity, the mean density structure would not be significantly perturbed. In addition, as will be seen below, a much more consistent and coherent pattern emerges from data analysis on constant-density surfaces than at constant-depth levels (e.g., Zhang and Levitus 1997). Such an analysis thus offers a new perspective on decadal thermocline variability around the North Pacific subtropical gyre. However, it is important to note that this straightforward interpolation method is different from an objective analysis scheme that projects hydrographic data directly onto isopycnal surfaces (e.g., Levitus 1989; Lozier et al. 1995).

3. The mean circulation structure and standard deviation of temperature anomalies

Figures 1a–c show mean depths of the 24.6, 25.2, and 25.6 kg m^{-3} isopycnal surfaces that are within the ventilated thermocline. The sloping of the isopycnals is clearly evident, with a zonally oriented trough–ridge structure. For example, on the 24.8 kg m^{-3} isopycnal surface (Fig. 1a), the maximum-depth regions lie between 15° and 25°N in the western Pacific and extend eastward to the central and eastern basin. A tropical trough extends westward from the eastern boundary across the basin along 10°N. On the 25.2 kg m^{-3} isopycnal surface (Fig. 1b), the regions of the greatest depths, as large as 200 m, are located south of the subtropical gyre at latitudes 15°–30°N in the western and central Pacific Ocean. On the 25.6 kg m^{-3} isopycnal surface (Fig. 1c), the deepest regions move northward to along 25°N. These isopycnals intersect the sea surface in the midlatitudes (outcropping), which, in our isopycnal analysis, is determined if the estimated depth of an isopycnal surface is less than 30 m.

To present the mean flow pattern, Figs. 1d–f show the Bernoulli function (B) evaluated on the 24.6, 25.2, and 25.6 kg m^{-3} isopycnal surfaces, respectively. Following Cox and Bryan (1984), B can be defined as

$$B(\boldsymbol{\sigma}) = \boldsymbol{\rho}_0 g \boldsymbol{\eta} + g \int_{z(\boldsymbol{\sigma})}^{0} [\boldsymbol{\rho} - \boldsymbol{\rho}(\boldsymbol{\sigma})]\, dZ,$$

where $\sigma = \rho - 1000$ is an isopycnal surface of interest (where ρ is in situ density in kg m^{-3} units), η is the dynamic height relative to 480 db, g is the acceleration of gravity, and ρ_o is the mean density. As defined, B is the geostrophic streamline that measures the geostrophic flow away from the equator. Comparisons between current fields and B in a simulation of the Pacific subtropical–tropical upper-ocean circulation (Rothstein et al. 1998) indicate that the orientation of the B contour coincides with the currents at the points, suggesting that B can provide flow paths throughout most of the domain.

There are three different water pathways around the subtropical gyre that originate from the midlatitude outcrop regions (Figs. 1d–f). One originates in the western and central part of the northern subtropical gyre west of 170°E and extends westward into the midlatitude western boundary. Farther to the east between 170°E and 160°W, the second pathway runs westward and southward into the low-latitude western boundary. The third pathway originates farther to the east and can be seen to penetrate into the Tropics through the ocean interior. Note that the isopycnal surfaces in Figs. 1d–f all have three types of geostrophic streamlines but at shallower depths, streamlines from the midlatitude outcrop regions are more likely to penetrate into the equator through the ocean interior. These results have been investigated in previous studies (e.g., McCreary and Lu 1994; Liu et al. 1994; Rothstein et al. 1998).

Figure 2 illustrates potential vorticity (Q) evaluated on the 24.6 and 25.6 kg m^{-3} isopycnal surfaces, respectively. As is well known (e.g., Talley 1988), Q not only reflects the thermocline structure, but also can give an indication of flow paths in that Q is conserved locally along flow streamlines. In the northwestern portion of the subtropical gyre, there is a pronounced minimum Q region in the middle thermocline (Talley 1988; Hautala and Roemmich 1998), which exhibits nearly homogenous Q fields over great spans, both in the vertical and in the horizontal, bounded by sharp Q gradients to the north and to the northeast (e.g., Fig. 2b). In the southeastern portion of the subtropical gyre, there is a maximum Q band along 10°–15°N that extends westward from the eastern boundary (Fig. 2a). Furthermore, as suggested by the open Q contours on the shallow surface (Fig. 2a), we can see a signature of the ventilated thermocline in the northeastern part of the gyre: low and high Q bands that connect to the outcrop regions where Q is set by mixed layer processes. In particular, a low Q band can be seen to extend from the midlatitude outcrop region at about 150°W southwestward around the subtropical gyre toward the western Tropics. This provides a path through which water mass anomalies at the sea surface can be subducted into the thermocline around the subtropical gyre (Luyten et al. 1983).

The calculated standard deviation of temperature anomalies on the 24.6, 25.2, and 25.6 kg m^{-3} isopycnals shows well-defined regions of large and small variability (Fig. 3). Three regions of large variability (centers) can be seen that reflect different forcing mechanisms. One is located along the eastern boundary, with a barotropic pattern in the upper thermocline. This appears to reflect a vertical displacement of the thermocline. The second center is located in the tropical western–central Pacific, which reflects the energetic interannual variability associated with El Niño in the Tropics. Another band of large variability, originating from the outcrop region in the central and eastern midlatitudes, extends southwestward around the subtropical gyre toward the western subtropics and Tropics. This apparently reflects the

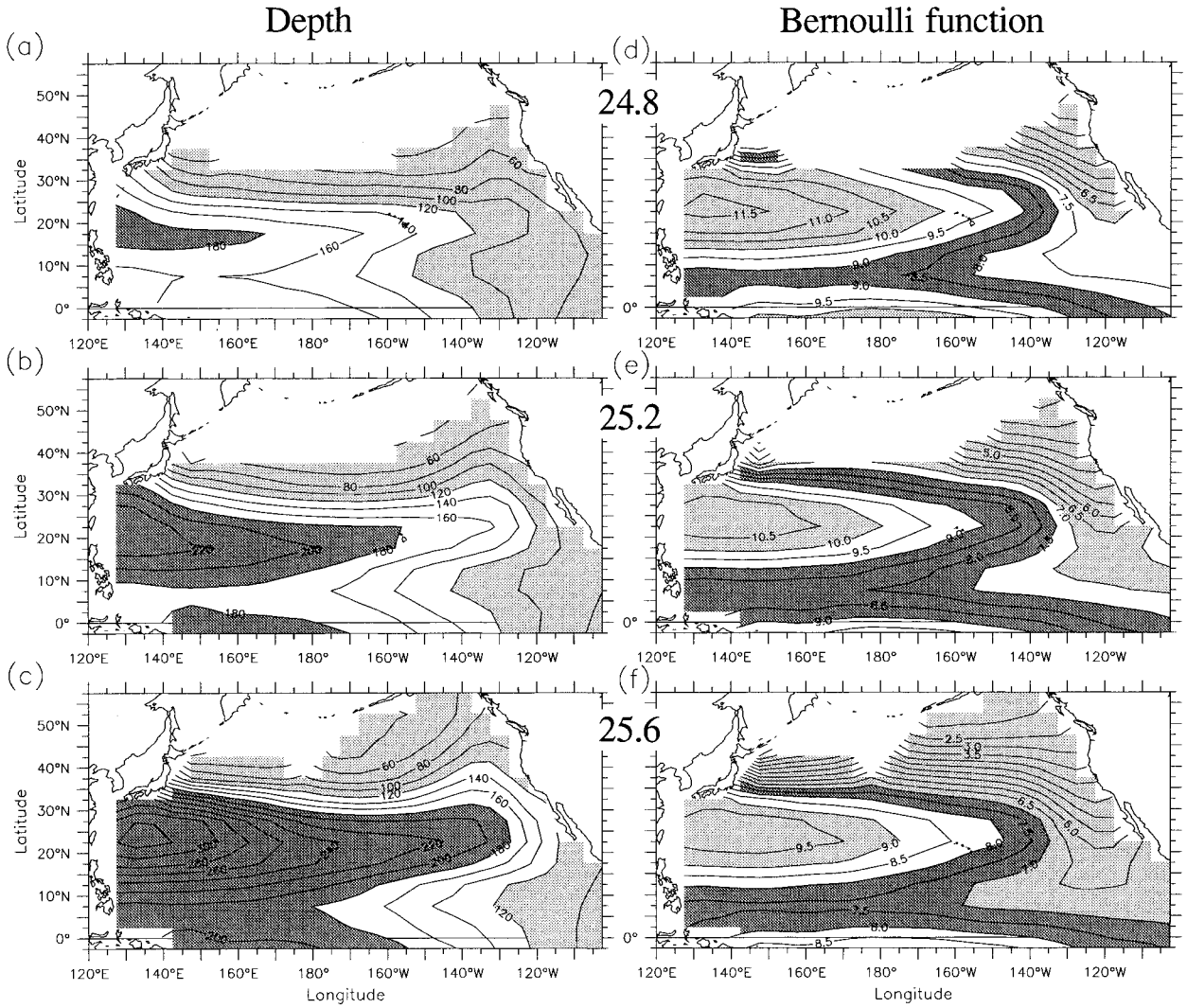

FIG. 1. (a)–(c) Mean depth and (d)–(f) Bernoulli function on the 24.8, 25.2, and 25.6 kg m^{-3} isopycnal surfaces, respectively. The contour interval is 20 m in (a)–(c) and 0.5 cm in (d)–(f).

ventilation of the subtropical gyre characterized by the subduction of sea surface temperature anomalies into the thermocline in the midlatitude outcrop region. On the 25.2 kg m^{-3} isopycnal surface (Fig. 3b), for example, a tail structure is clearly evident around the subtropical gyre, with a tongue of large variability originating from the sea surface and rotating downward and southwestward toward the western Tropics. A similar gyrelike pattern can be seen on deeper surfaces (e.g., Fig. 3c). On the 26.0 kg m^{-3} isopycnal surface (Fig. 3d), we can see a gyre-scale band of large variability that circulates from high latitudes at 60°N, 170°E southeastward to about 45°N, 160°W and then extends southwestward into the western Tropics.

There are two main regions of low variability. One is located in the western subtropics, with an east–west-oriented band at 20°–35°N; this appears to reflect the unventilated thermocline around the center of the subtropical gyre (Luyten et al. 1983; Liu 1996). Another band lies to the east of the large subduction variability region (but away from the boundary region of large variability). This may reflect the signature of the unventilated thermocline associated with the shadow regime in the eastern part of the subtropical gyre (e.g., Luyten et al. 1983; Liu 1996).

4. Thermocline variability on isopycnal surfaces

A large number of horizontal maps and vertical sections can be presented on isopycnal surfaces to give a three-dimensional picture of decadal thermocline variability in the North Pacific Ocean. Decadal events are clearly evident in the midlatitudes during the analyzed period: a warm phase in the 1960s and early 1970s, a cold phase in the late 1970s and 1980s, a transition from the warm to cold conditions in the mid-1970s, and pos-

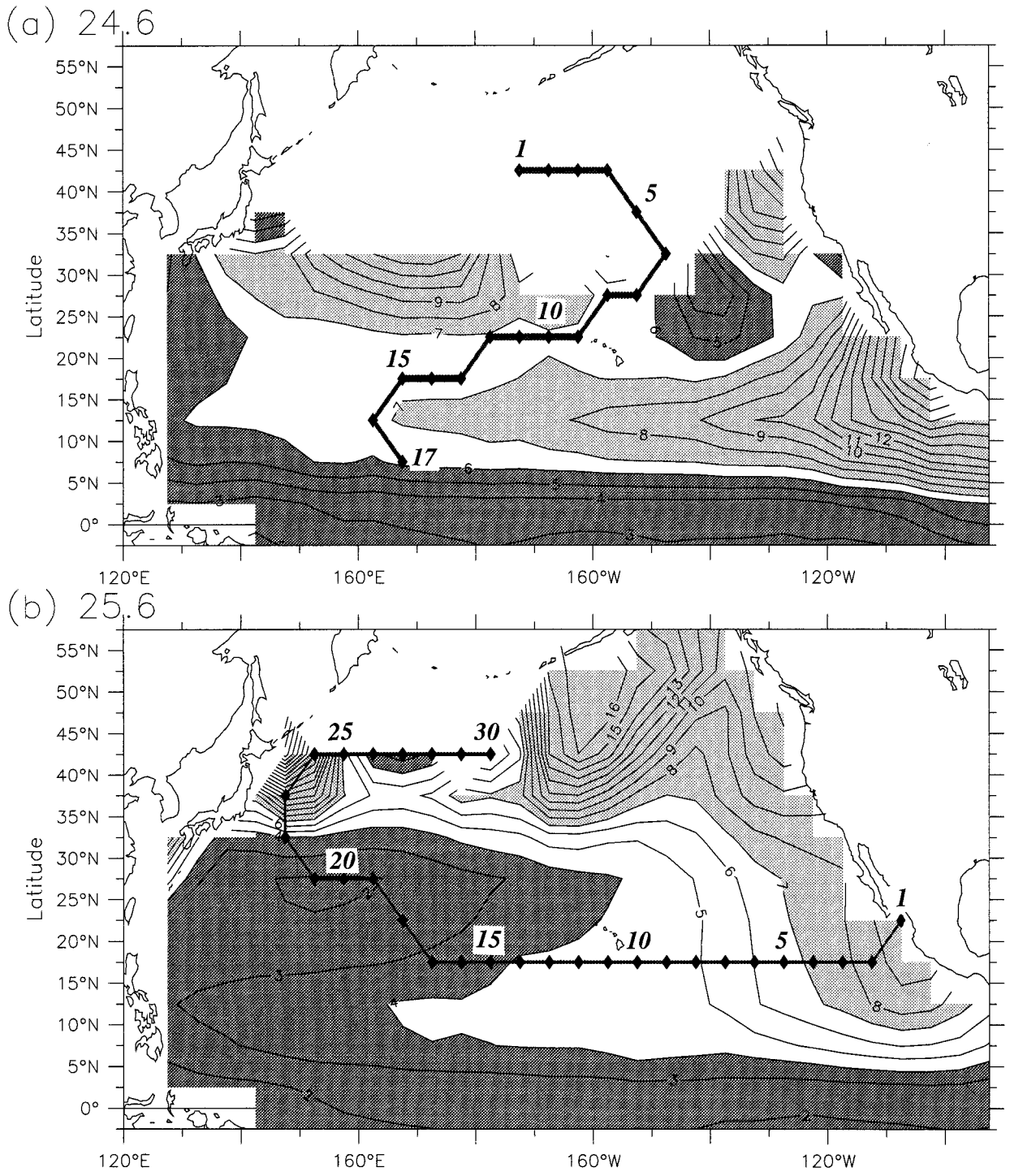

FIG. 2. Potential vorticity evaluated on the (a) 24.6 and (b) 25.6 kg m^{-3} isopycnal surfaces. The contour interval is 1×10^{-10} m^{-1} s^{-1}. The two heavy lines with diamond marks indicate (a) the southwestward subduction pathway and (b) the westward subtropical pathway.

sibly another transition from cold to warm conditions in the late 1980s. Compared with previous data analyses performed at constant-depth levels (e.g., Deser et al. 1996; Zhang and Levitus 1997), this new analysis on constant-density surfaces demonstrates a coherent relationship of decadal thermocline variability around the North Pacific subtropical gyre more clearly.

Two major preferential pathways can be identified that are associated with decadal thermocline variability around the subtropical gyre on decadal timescales. One

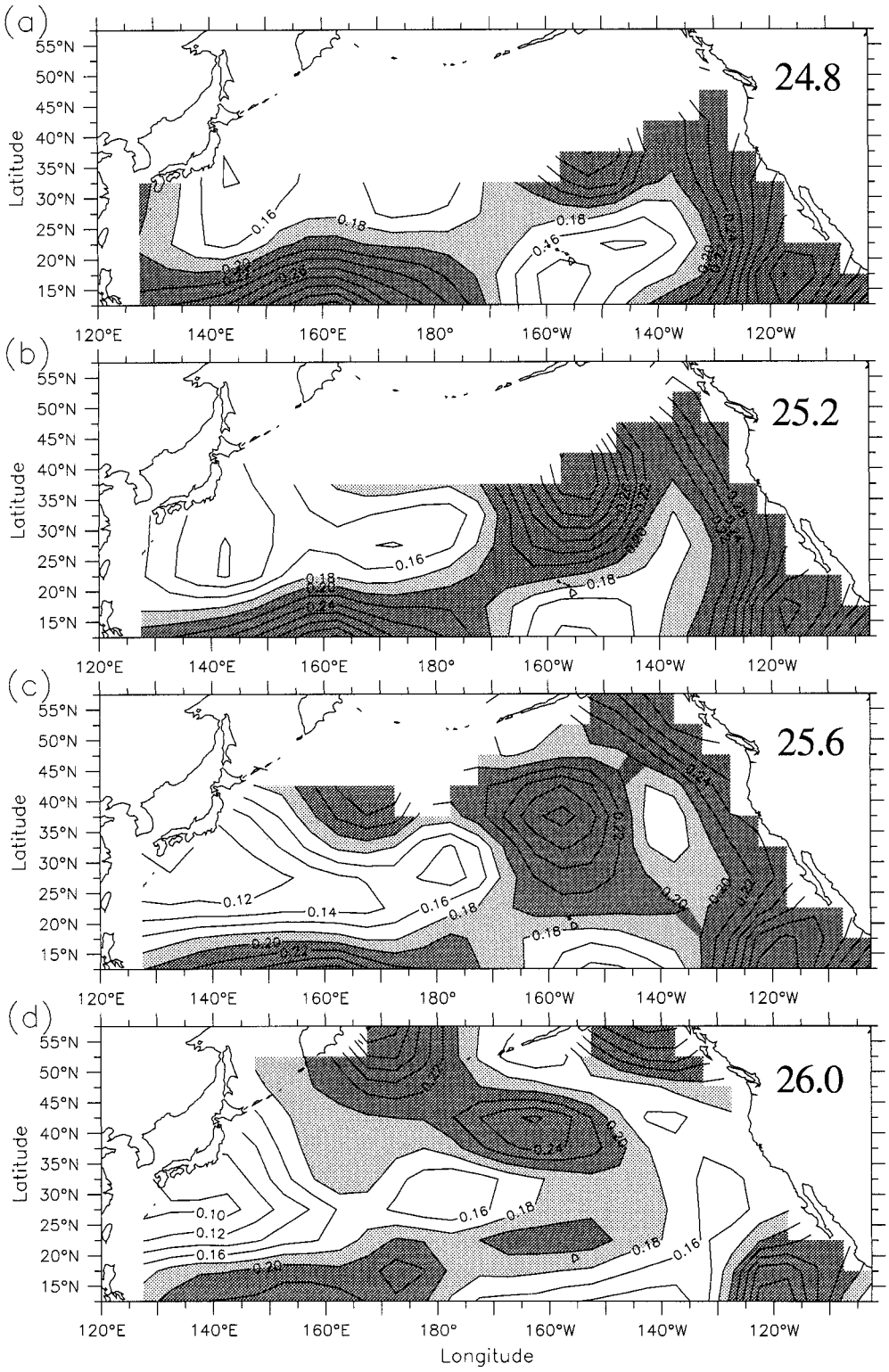

FIG. 3. Horizontal distribution of the standard deviation for temperature anomalies on the (a) 24.8, (b) 25.2, (c) 25.6, and (d) 26.0 kg m^{-3} isopycnal surfaces in the North Pacific Ocean. The contour interval is 0.02°C.

dominant pathway originates from the outcrop region in the northeastern part of the gyre centered at about 40°N, 150°W and extends southwestward along the low *Q* region (Fig. 2a) toward the western subtropics and Tropics, a clear signature of the ventilated thermocline. This, therefore, can be physically interpreted as a subduction pathway. Another pathway extends from the eastern subtropics–Tropics and boundary regions and appears to continue predominantly westward across the southern part of the gyre (between 15° and 30°N) and then along the Kuroshio path toward the midlatitudes. Since the horizontal propagation of thermocline anomalies is mostly pronounced and significant in the subtropics on decadal timescales, we simply call it a subtropical pathway. In Fig. 2, we schematically illustrate the two pathways. The choice of the locations is based on the preferential appearance of temperature anomalies along these two paths and also on the results of EOF analyses to be shown below.

Temperature anomalies along the two pathways are shown in Fig. 4 as a function of time and distance on some isopycnals. Along the subduction pathway, we show only one isopycnal surface (Fig. 4b) because other isopycnals basically have similar patterns; along the subtropical pathway, we show two isopycnals (Figs. 4a,c) in order to illustrate the differences in the vertical structure of temperature anomalies in the upper and lower portions of the thermocline.

a. The (southwestward) subduction pathway

Two subduction events (one warm, one cold) are apparent in Fig. 4b. A midlatitude warm temperature anomaly observed in the early 1970s appears to extend southward and westward, penetrating through the subtropics into the western Tropics in the mid- and late 1970s (Zhang et al. 1998). Similarly, a midlatitude cold anomaly observed in the early 1980s can be traced to the subtropics and Tropics as a subducted signal (e.g., Deser et al. 1996). The detailed pathways of these two subduction events around the basin are shown in Fig. 5 for temperature anomalies on the 25.0 kg m^{-3} isopycnal surface for two periods 1973–78 and 1983–88, respectively. These two periods also correspond to decadal phase transitions in the midlatitudes occurring in the mid-1970s and in the late 1980s, respectively. The contours of *B,* which define the geostrophic flow relative to 480 db, are superimposed in Fig. 5a to indicate the fluid trajectories.

The thermocline anomalies appear to be well organized into a coherent pattern by the ventilation of the subtropical gyre, characterized by a clockwise rotation from the midlatitude outcrop regions to the central and western subtropics and Tropics (Fig. 5). In the 1960s through the mid-1970s, the North Pacific Ocean was in a warm phase, with a warm sea surface temperature anomaly in the central midlatitudes. In early 1970s (e.g., Fig. 5a), a warm temperature anomaly emerged on the 25.0 kg m^{-3} isopycnal in the midlatitude outcrop region approximately at 40°N, 150°W, surrounded by negative anomalies in the subtropics (Fig 5a). Thereafter, a tongue can be seen to extend from the outcrop areas downward and southward; surface anomalies appeared to be subducted into the thermocline. The subducted anomalies then followed approximately the mean circulation (see *B* contours in Fig. 5a) and were swept southwestward on isopycnals toward the western subtropics and Tropics. Some parts appeared to penetrate into the Tropics in the central Pacific (Zhang et al. 1998). A similar pattern can be seen during 1983–88 (right panels in Fig. 5) but with the opposite sign of temperature anomalies. Figure 5g illustrates the emergence of a cold anomaly in the midlatitude outcrop region in 1983, representing the initial stage of its subsequent subduction into the thermocline (Figs. 5h–k). Thereafter, the cold anomaly was subducted into the thermocline along isopycnals and through the northwest of Hawaii, and continued to move southwestward around the gyre into the western subtropics and Tropics. The latter subduction case was first illustrated by Deser et al. (1996).

The downward and southward movements of temperature anomalies are further illustrated in the meridional sections along 157.5°W for the years 1968–90 (Fig. 6). During the early 1970s, a major warm anomaly can be observed to form in the surface layer (e.g., Fig. 6c); with time, the anomaly became detached from the surface and was subducted downward into the thermocline, and then it progressed southward on isopycnals centered near the 25.1 density surface. In the mid- and late 1970s (Figs. 6e–f), the warm anomaly was located in the subtropics, and some extended upward in the Tropics, losing their identity thereafter. At the same time, a negative anomaly first emerged at high-latitude subsurface depths in the late 1970s (Fig. 6e) and then extended southward and upward in the midlatitudes. By 1978 (Fig. 6f), the negative anomaly extended subsurface to the 25.4 kg m^{-3} isopycnal surface; by 1982 (Fig. 6h), it extended subsurface from the 26.2 to 25.0 kg m^{-3} isopycnal surfaces in the subtropics. This anomaly was apparently not directly generated by local surface layer processes, but appeared to be a signal that had extended from the northwestern midlatitude regions. In the early 1980s, a significant cold anomaly developed in the surface layer (Fig. 6i). Thereafter, these two (subsurface- and surface-originated) anomalies appeared to have combined and progressed southward and westward on isopycnal surfaces, becoming detached from the surface and penetrating into the Tropics. Similarly, in the late 1980s, a subsurface positive anomaly first emerged in the thermocline in the midlatitudes (Fig. 6l). This anomaly is clearly associated with a wave signal in the subtropics that can be traced to the eastern tropical boundary in the early 1980s (e.g., Figs. 5g–h).

b. The (westward) subtropical pathway

Two examples of coherent trans-Pacific westward propagation of thermocline anomalies can be seen in

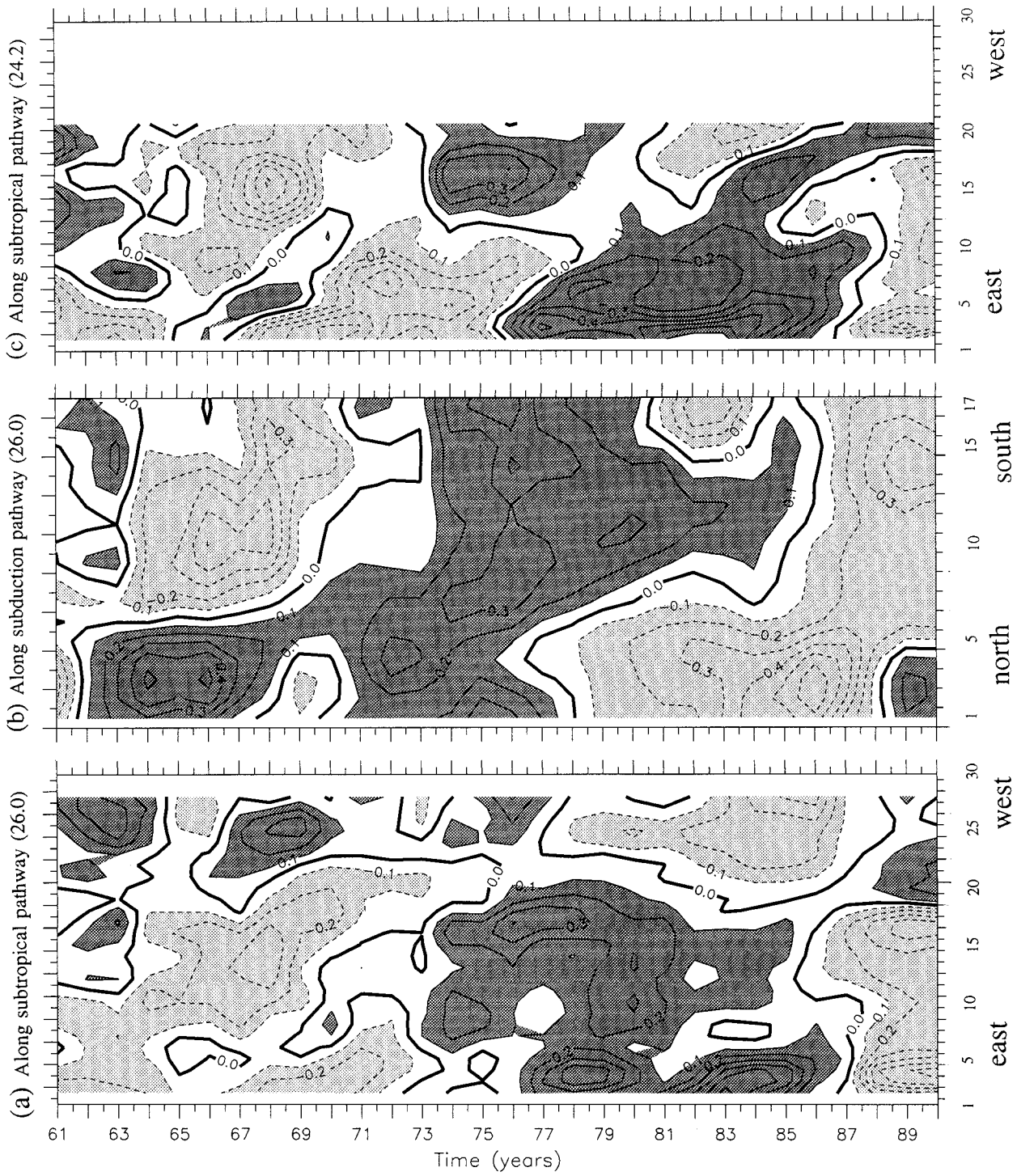

FIG. 4. Temperature anomalies as a function of time and distance along the subtropical pathway on the (a) 26.0 and (c) 24.2 kg m^{-3} isopycnal surfaces and along the subduction pathway on the (b) 26.0 kg m^{-3} isopycnal surface. The contour interval is 0.1°C with the dashed line for negative anomalies. The horizontal axis gives the line segments that are displayed in Fig. 2 (in numbers): from the east to west in (a) and (c), and from the north to south in (b).

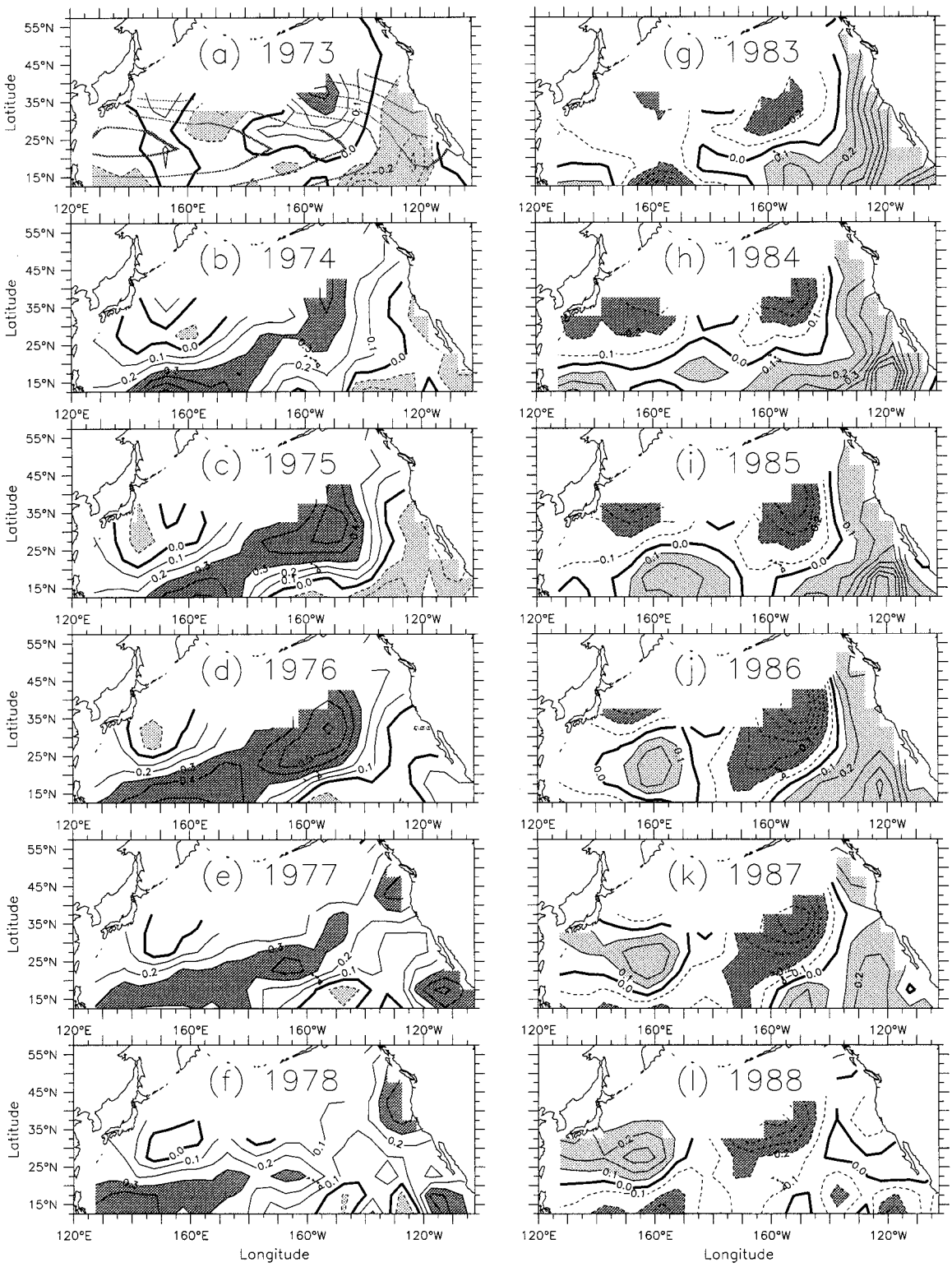

FIG. 5. Horizontal distribution of temperature anomalies (contour interval is 0.1°C) on the 25.0 isopycnal surface for the years 1973–78 (left panels) and for the years 1983–88 (right panels). Superimposed is the Bernoulli function evaluated on the 25.0 kg m^{-3} isopycnal surface in (a) (the shaded line; contour interval is 0.5 cm).

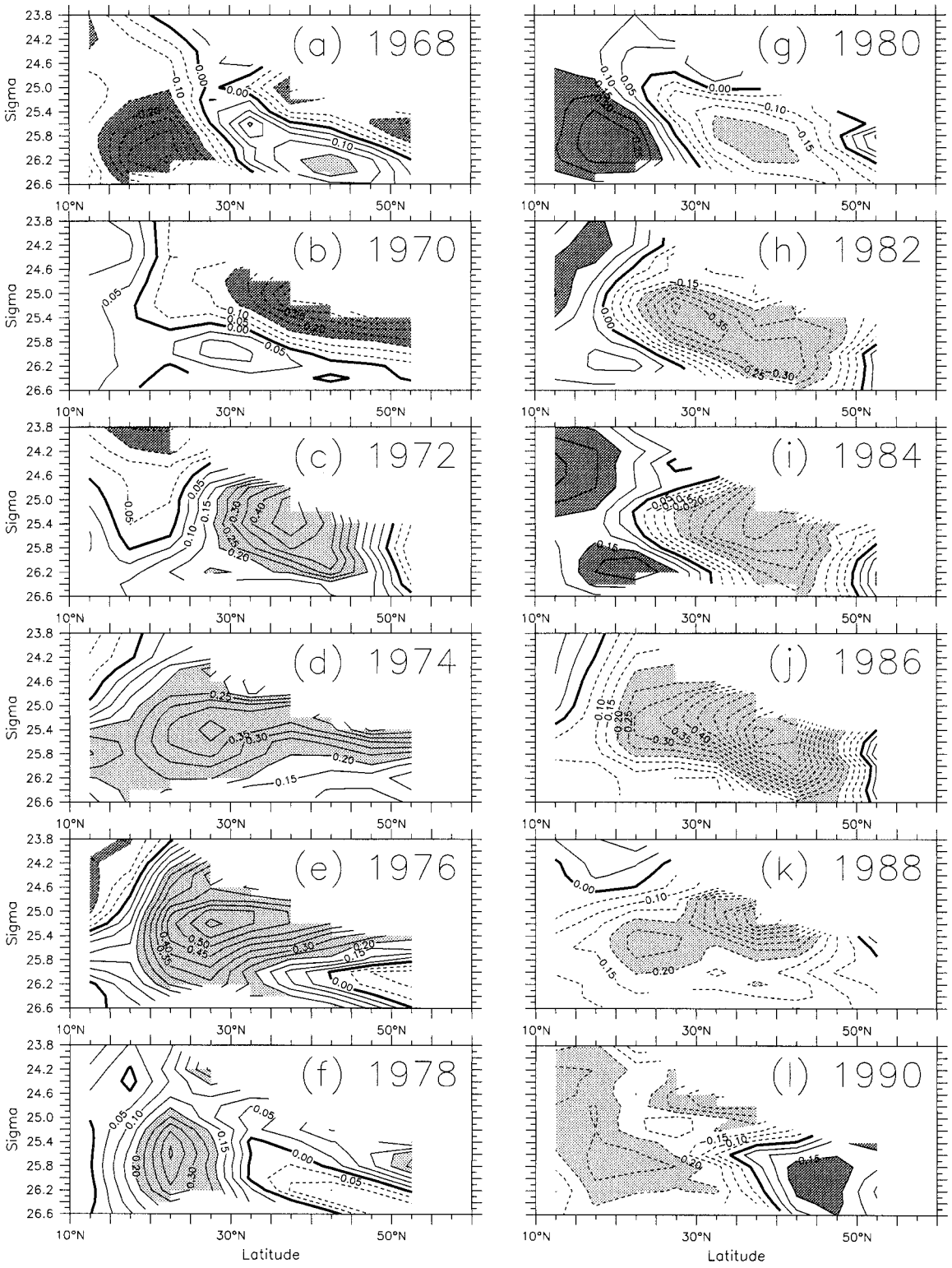

FIG. 6. Meridional sections of temperature anomalies along 157.5°W for the years 1968–90. The contour interval is 0.05°C with the dashed line for negative anomalies.

Figs. 4a and 4c: a negative anomaly in the late 1960s and a positive anomaly in the 1980s that have respectively extended across the entire basin on decadal timescales. This signal is most pronounced and significant in the subtropics. Figure 7 shows temperature anomalies as a function of isopycnal surface and time for three different sites in the eastern subtropics–Tropics and boundary regions (i.e., the source regions of the subtropical pathway). Decadal changes are clearly evident, characterized by a phase transition from negative to positive anomalies in the mid- and late 1970s. A barotropic vertical structure is apparent in the upper thermocline between the 23.8 and 26.0 kg m^{-3} isopycnal surfaces, suggesting that the signal can be mainly attributed to a vertical displacement of the thermocline forced by wind stress curl. The temperature anomaly signal then appeared to propagate westward and upward along the subtropics.

Figure 8 presents the vertical structure of temperature anomalies as a function of isopycnal surface and distance along the subtropical pathway for the two periods 1965–70 and 1981–86, respectively. In the 1960s, large negative anomalies were present in the eastern boundaries. At deep layers, a negative temperature anomaly signal, originating from the eastern boundary, propagated very slowly westward across the basin primarily along the 26.0 kg m^{-3} isopycnal surface (also see Fig. 4a) and then extended upward in the central and western subtropics. The propagation speed (about 0.1 cm s^{-1} in the central basin but much faster, more than 1 cm s^{-1}, in the eastern and western regions was too slow to be a first-mode Rossby wave, but the signal could have been a higher-mode Rossby wave or simply advected by mean flow (Liu 1999a,b). In the shallow layer, a negative temperature anomaly signal propagated westward across the basin from the eastern boundary in the late 1960s and in the early 1970s (also see Fig. 4c) to the central and western subtropics; there, the signal appeared to be locally amplified, probably by wind forcing. This signal then continued to propagate through the Kuroshio region and arrived in the western and central midlatitudes in the early 1970s (Figs. 4c and 8f).

A more clear example of a propagating signal along the subtropical pathway is evident in the 1980s. Associated with the decadal transition in the late 1970s, positive temperature anomalies can be seen in the eastern Tropics and coastal regions (Fig. 4c). Figure 5 has shown the basinwide evolution of a positive temperature anomaly signal on the 25.0 kg m^{-3} isopycnal surface across the subtropical basin (right panels). This signal appears to have originated from the eastern tropical boundary and, at a speed of about 2 cm s^{-1}, has propagated westward from the eastern basin (about 150°W) in 1983 (Fig. 5g) to the western subtropics (about 155°E) in 1988 (Fig. 5l) and then continued its way along the Kuroshio path. In the late 1980s, the decade-long cold state in the North Pacific appeared to be reversing: a strikingly positive anomaly was located in the western Pacific along 25°–38°N, accompanied by negative anomalies in the subtropics and along the eastern boundary (Fig. 5l).

For the years 1981–86, the vertical structure of thermocline anomalies along the subtropical pathway can be seen in the right panels of Fig. 8. Compared with that in the 1960s (the left panels), a similar but reverse pattern is evident. At a deep layer on the 26.0 kg m^{-3} isopycnal surface, a positive temperature anomaly signal propagated predominantly westward across the southern part of the subtropical gyre (between 15° and 30°N), accompanied by a fast propagating signal of a positive temperature anomaly at a shallow layer as a radiating Rossby wave from the eastern boundary (Jacobs et al. 1994). In the western subtropics, these two signals appeared to combine together and continued to propagate along the Kuroshio path toward the midlatitudes. The decadal westward propagation across the Pacific subtropical basin in the 1980s, as seen from the in situ subsurface temperature observations in this study, has been investigated by Jacobs et al. (1994) from other data sources.

Temperature anomaly signals along the subtropical pathway appear to involve different mechanisms. As shown in the horizontal maps (e.g., the right panels in Fig. 5), the propagation direction of the positive temperature anomaly signal deviates significantly from the mean circulation presented by the B contours (Figs. 1d–f), with anomalies extending upward when moving through the western subtropics (i.e., not necessarily along one isopycnal surface). In addition, the anomaly source regions appear to be located in the eastern subtropical–tropical boundaries and be related to wind forcing (e.g., Liu 1993). Thus, the coherent westward propagation along the subtropical pathway can be physically ascribed to Rossby waves (e.g., Liu 1999a,b), which have been previously identified in surface height (e.g., Jacobs et al. 1994; Chelton and Schlax 1996). On the other hand, some anomaly signals along the subtropical pathway can indeed be attributed to subduction mechanism. For example, a midbasin positive anomaly observed in the mid-1970s (Fig. 4c) was a subducted anomaly from the midlatitude outcrop region (Fig. 4b). On the 26.0 kg m^{-3} isopycnal surface (Fig. 4a), a midbasin positive anomaly observed in the early 1970s appeared to be of subduction origin as well, with a clear signature at the shallow layer along the subduction pathway (figures not shown). But it is evident that these subducted anomalies do not show consistent trans-Pacific propagation along the subtropics. In addition, there is an indication of intensification when an anomaly propagated through the central and western subtropics, suggesting that decadal changes in the wind stress or Ekman pumping fields may have been involved (e.g., Miller et al. 1998; Deser et al. 1999).

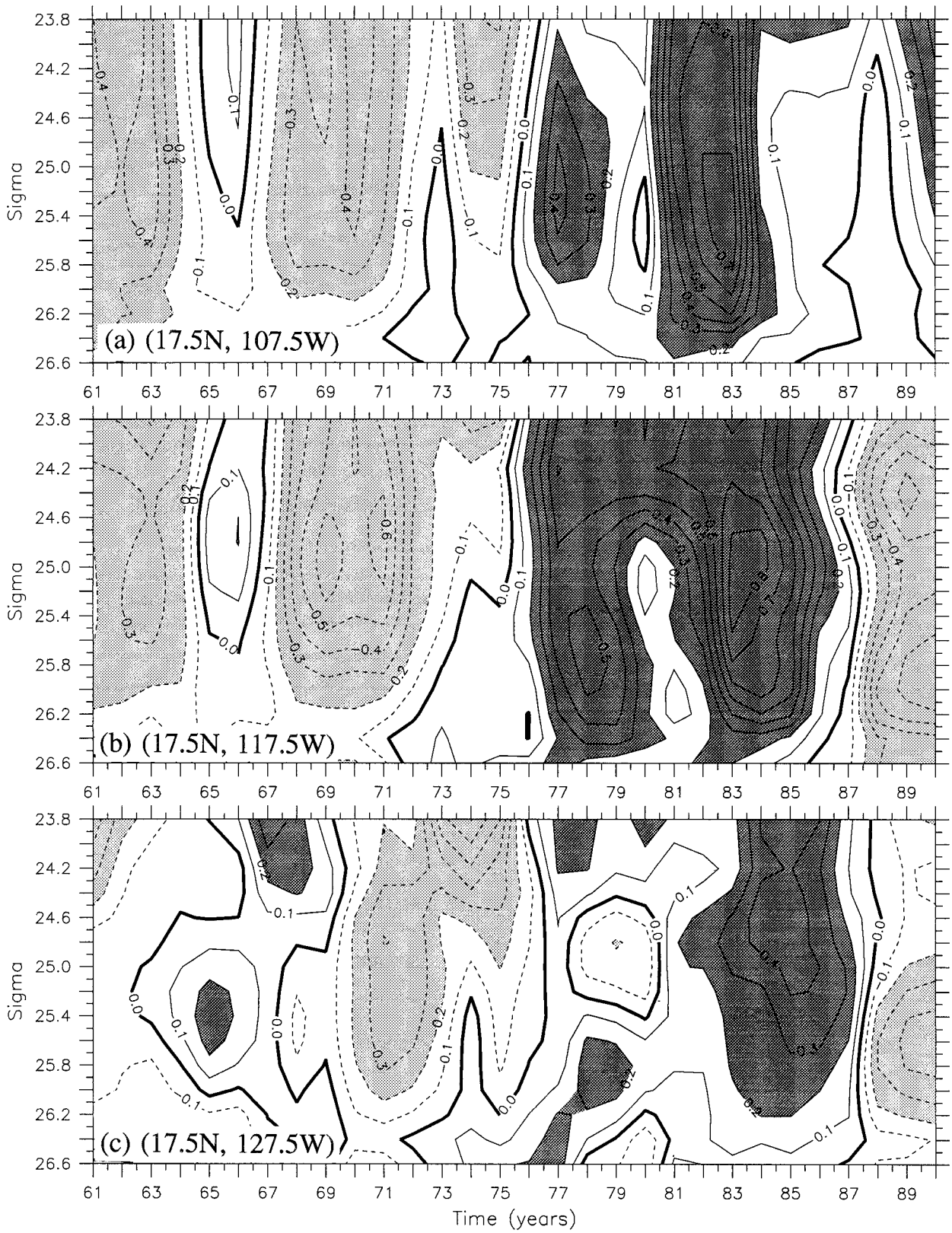

FIG. 7. Temperature anomalies as a function of isopycnal surface and time for three different regions along the subtropical pathway at (a) 17.5°N, 107.5°W, (b) 17.5°N, 117.5°W, and (c) 17.5°N, 127.5°W. The contour interval is 0.1°C with the dashed line for negative anomalies.

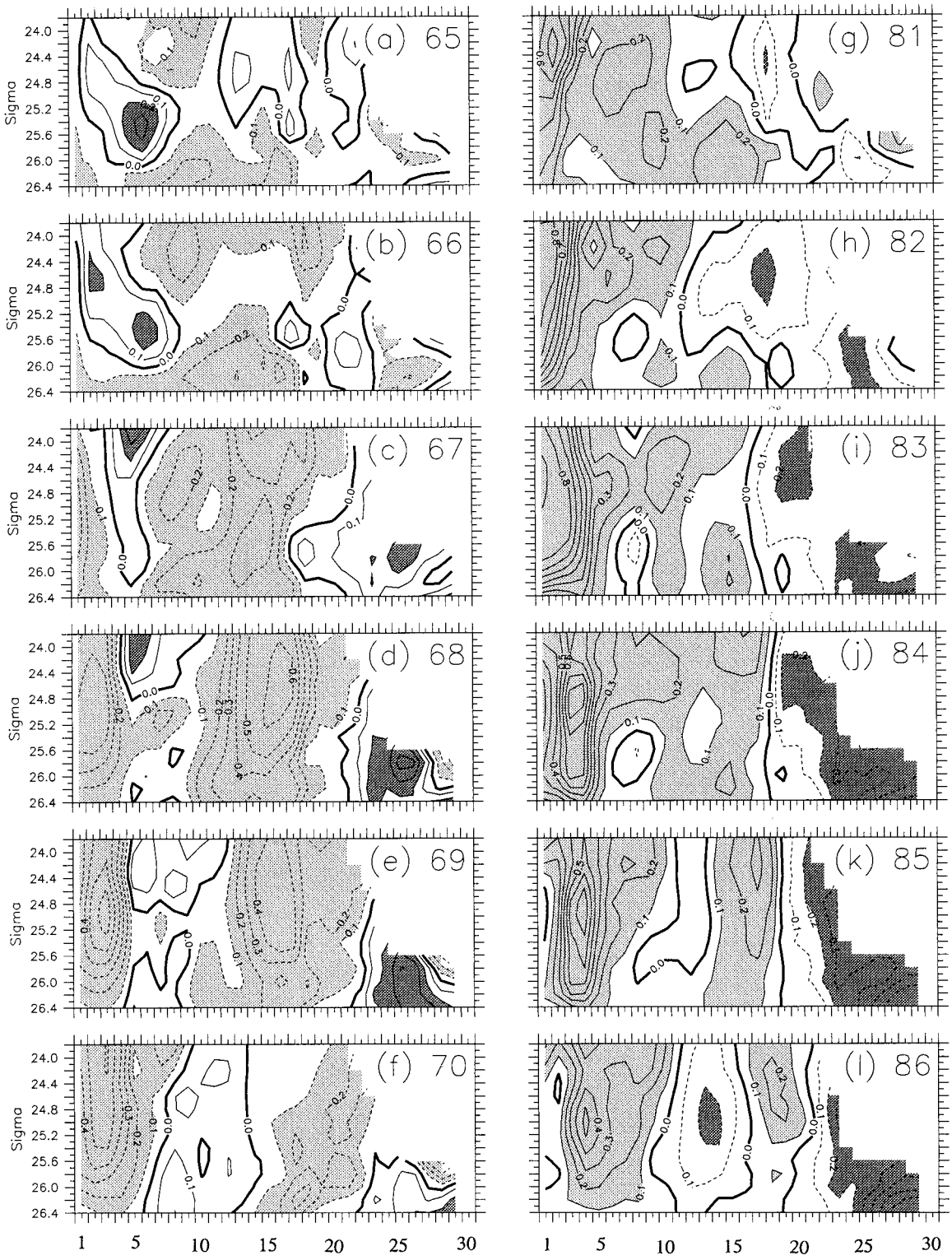

FIG. 8. Temperature anomalies as a function of isopycnal surface and distance along the subtropical pathway for the years 1965–70 (left panels) and for the years 1981–86 (right panels). The horizontal axis gives the line segments displayed in Fig. 2 as indicated in the numbers. The contour interval is 0.1°C with the dashed line for negative anomalies.

c. Relationships of thermocline variability along the subtropical gyre

Thermocline anomalies associated with the two pathways appear to have consistent phase relationship to one another around the North Pacific subtropical gyre. Anomalies in the source regions of the two pathways (one in the midlatitude outcrop region and the other in the eastern subtropics–Tropics and boundary regions) tend to be out of phase (Fig. 4). In the 1960s, a negative temperature anomaly signal propagated across the subtropics and continued toward the midlatitudes through the early 1970s, followed by a subducted warm anomaly that originated from the midlatitude outcrop region in the early 1970s and penetrated into the central and western subtropics–Tropics in the mid- and late 1970s. Similarly, in the late 1970s and early 1980s, a positive temperature anomaly signal started to propagate westward from the eastern boundary and crossed the subtropical basin during the 1980s, followed by a subducted cold anomaly from the midlatitudes in the early 1980s. As a result, thermocline variability around the North Pacific subtropical gyre appears to be alternately dominated by two different dynamical signals on decadal timescales: the subduction around the northeastern to southwestern part of the gyre and the trans-Pacific westward propagation in the subtropics. In addition, there is a visual continuity of thermocline anomalies along the subduction pathway and along the subtropical pathway (Fig. 4), suggesting a possible connection between thermocline variability around the subtropical gyre.

5. An EOF analysis

In order to detect the dominant structure and time variations, we perform an empirical orthogonal function (EOF) analysis of temperature anomaly fields on all isopycnal surfaces of 23.8–26.4 kg m^{-3} in increments of 0.2 kg m^{-3} (see the appendix for a brief description of EOF analysis). To illustrate the differences of temperature variations in the surface layer and in the thermocline, we also perform an EOF analysis for surface-layer temperature anomalies. To be consistent with the outcrop determination of an isopycnal (i.e., whether or not its depth is less than 30 m), we obtained surface-layer anomalies by averaging temperature anomaly fields at depths of 0, 10, 20, and 30 m, respectively. This can also present the well-mixed nature of temperature variations in the surface layer.

The horizontal domain of our analysis is the 7.5°–62.5°N region of the North Pacific Ocean. The EOFs are computed based on a covariance matrix for 30 yr from 1961 to 1990. Table 1 presents fractional variances for the surface layer and for each isopycnal surface explained by the first three EOF modes. To identify the statistically significant EOFs, we adopt the procedure recommended by North et al. (1982) to check if the sampling error of a given eigenvalue is smaller than the spacing between the eigenvalue and a neighboring eigenvalue. The results indicate that the first two EOFs have much smaller sampling errors and definitely pass such a rule of thumb test.

TABLE 1. Fractional variances for each layer explained by the first three EOF modes. The results for the combined EOF analysis performed on the whole upper ocean are also given.

Layers (kgm m^{-3})	Modes (%)			Cumulative (%)
	EOF 1	EOF 2	EOF 3	
Surface	34.1	16.0	11.8	61.9
23.8	38.5	23.0	9.4	70.9
24.2	37.3	24.6	9.2	71.1
24.4	37.2	25.8	9.5	72.5
24.6	35.3	28.8	8.8	72.9
24.8	33.3	29.6	8.4	71.3
25.0	33.7	29.4	8.4	71.5
25.2	33.7	29.4	8.1	71.2
25.4	34.8	28.2	8.3	71.3
25.6	35.7	25.5	9.2	70.4
25.8	37.6	23.6	8.7	69.9
26.0	36.8	24.8	7.5	69.1
26.2	40.1	22.4	9.7	72.2
26.4	40.2	22.4	13.0	75.6
Mean	36.3	25.3	9.3	70.8
Combined EOF	30.5	25.9	8.9	65.3

a. Principal structure on isopycnal surfaces

The results of EOF analysis for temperature in the surface layer (not shown) are similar to other previous studies (e.g., Graham 1994; Miller et al. 1994; Trenberth and Hurrel 1994). On the 25.2 kg m^{-3} isopycnal surface (Fig. 9), the time coefficients of the first two EOF modes clearly indicate decadal-scale variations, with coherent phase relationships to one another (Fig. 9a). The first mode (solid line) exhibits a large positive anomaly period in the 1960s and 1970s, with a sharp phase transition to a negative anomaly in the late 1970s. The second mode (dashed line) also shows decadal changes, lagging the first by several years. The spatial patterns of the first EOF mode (Fig. 9b) are indicative of the ventilated thermocline and of gyre circulation structure. We can see a tongue of positive anomaly that originates from the midlatitude outcrop region at about 40°N, 150°W and extends southward and westward in the direction of the gyre flow (see the Bernoulli contours in Fig. 1). This pattern clearly represents the two subduction events as have been illustrated in Fig. 5. This mode also has a large negative anomaly in the eastern subtropics and along the North American coastal regions. After several years, the spatial patterns are described by the second mode (Fig. 9c). At this time, a large positive anomaly is located in the western Tropics and along the North American coastal regions.

Down to the 26.0 kg m^{-3} isopycnal surface (Fig. 10), the first two principal components indicate a coherent phase relation, with the first leading the second by several years (Fig. 10a). Compared to those on the 25.2 kg

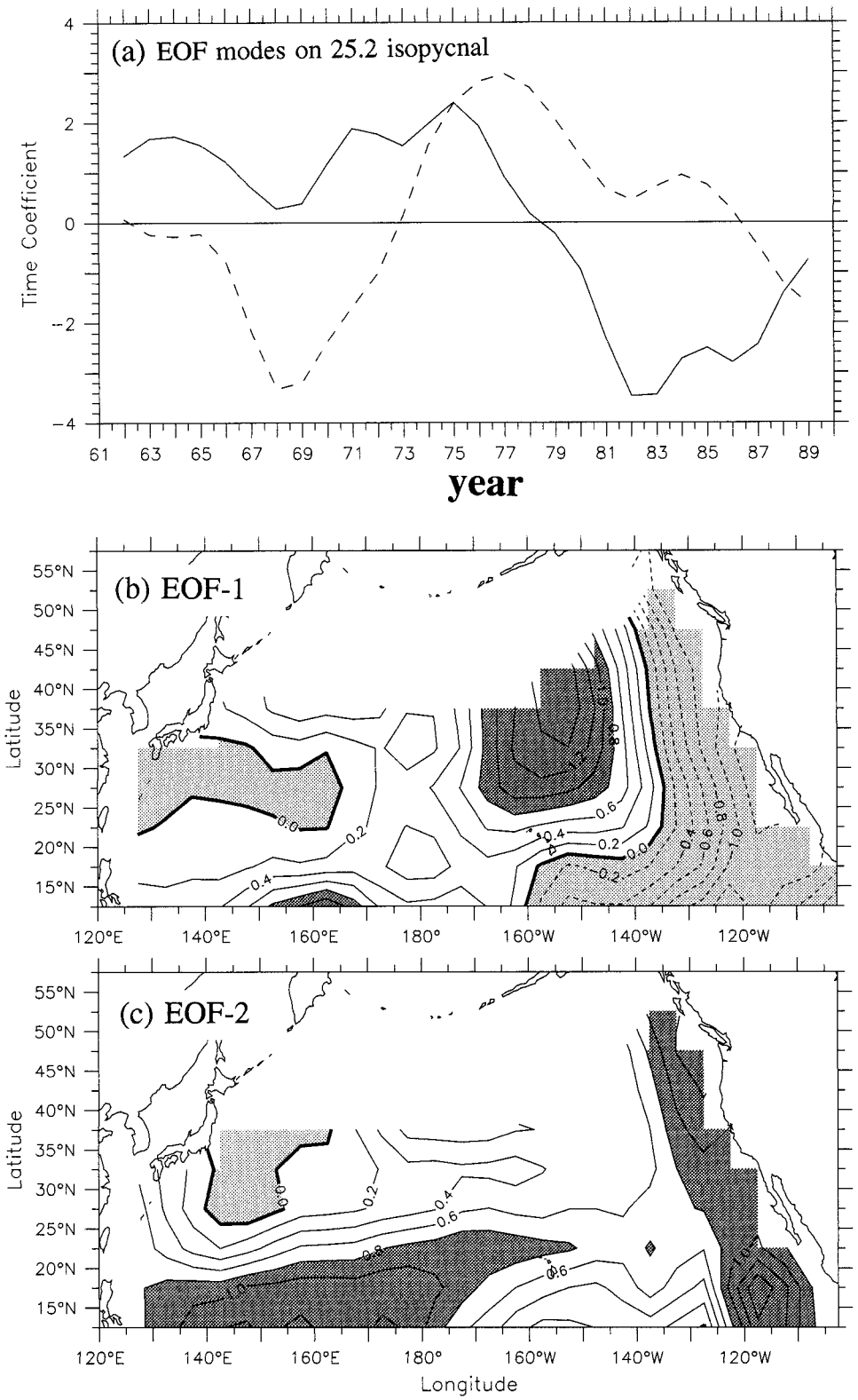

FIG. 9. Time variations and spatial patterns of the first two EOF modes for temperature anomalies on the 25.2 kg m^{-3} isopycnal surface. (a) The solid line for the first mode and the dashed line for the second mode, (b) the first eigenvector, (c) the second eigenvector. Contours in the eigenvector figures show the actual eigenvector value multiplied by 10. The contour interval is 0.2 with the dashed line for negative areas.

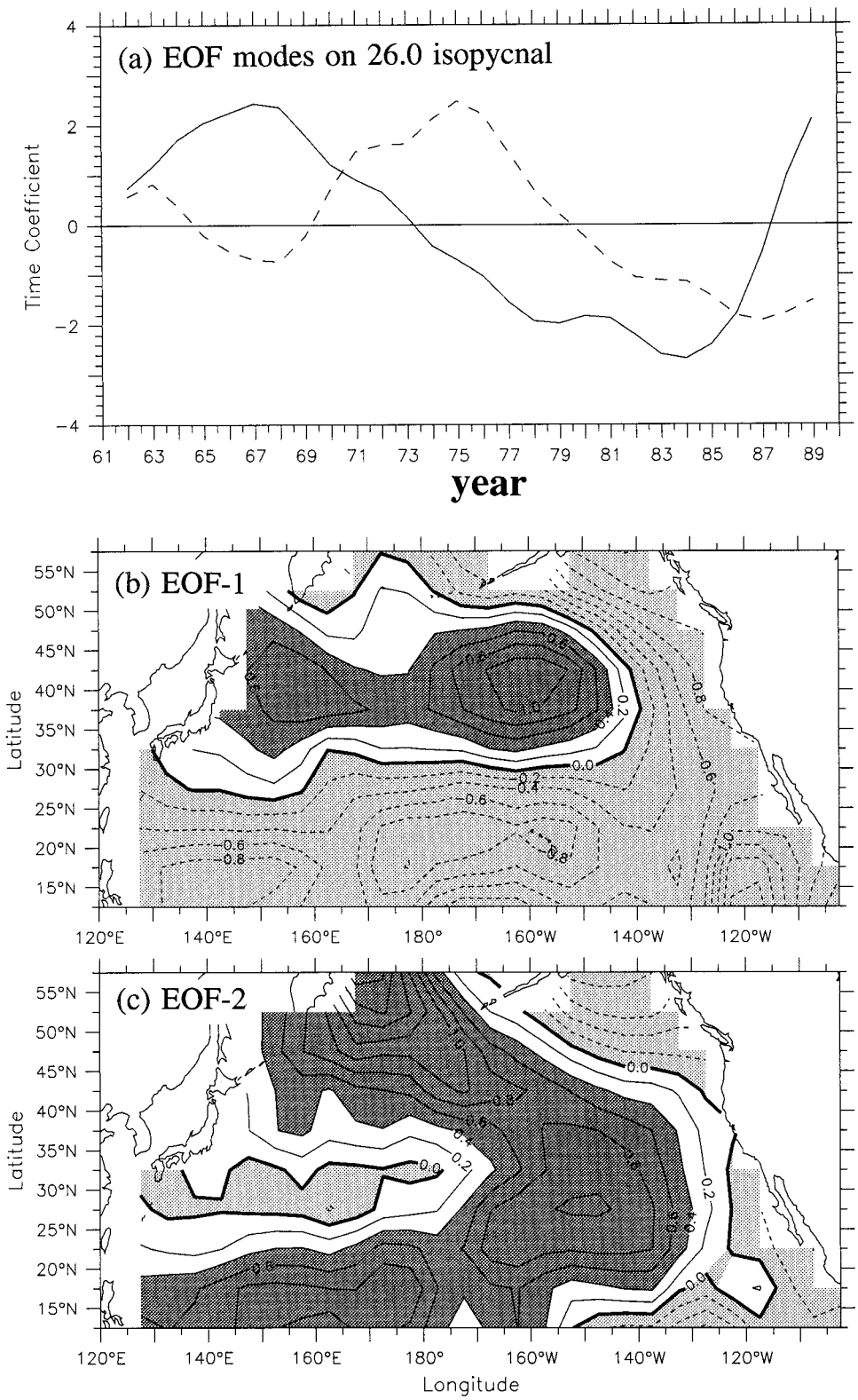

FIG. 10. The same as in Fig. 9 but for temperature anomalies on the 26.0 kg m^{-3} isopycnal surface.

m^{-3} isopycnal surface, the dominant spatial patterns change significantly on this isopycnal. The first mode (Fig. 10b) is characterized by two zonal bands of the opposite sign: a seesaw structure in the midlatitudes (about 40°N) and in the subtropics (about 20°N). When a positive anomaly is located in the north, a negative anomaly band tends to be located in the subtropics and along the North American coastal regions. The second mode (Fig. 10c) is characterized by a gyre-scale band of positive anomaly that extends from high latitudes at 60°N, 170°E southeastward to about 45°N, 160°W and then rotates southwestward to the western Tropics. There is a small negative anomaly along the eastern boundary region and in the western subtropics at 30°N.

b. Combined structure

The separate EOF analyses performed above on each layer clearly show the structural and phase differences in temperature variations in the surface layer and in the thermocline. In order to provide information on a vertically consistent pattern and on the coherent relationship between surface and thermocline variability, a combined EOF analysis is performed on the entire North Pacific upper ocean spanning 7.5° to 62.5°N (e.g., Zhang and Levitus 1997). In so doing, all temperature anomaly data in the surface layer, and on isopycnals of 23.8, and of 24.2–26.4 kg m^{-3} in increments of 0.2 kg m^{-3} (a total of 14 layers), are included simultaneously in the covariance matrix from which the dominant time variations and spatial patterns are detected (see the appendix). Thus, each EOF mode on different layers has similar time variations but can have different spatial patterns. This technique can reveal the dominant patterns of the three-dimensional upper-ocean thermocline variability in a consistent way.

The first three combined EOFs explain about 31%, 26%, and 9% of the total variance, respectively (Table 1). Figure 11a depicts the time series of the amplitude for the first two combined EOF modes. The first mode (the solid line) clearly shows the 1976–77 climate transition in the North Pacific Ocean, from a warm to a cold state. The transition condition from the decadal warm to cold anomalies is described by the second EOF mode, which has the maximum amplitude around 1976–77 (the dashed line).

The spatial patterns depicted by the combined EOF analyses (Fig. 12) show coherent relationships between temperature variations at the sea surface and in the thermocline around the North Pacific subtropical gyre. The first mode (Fig. 12, left panels) indicates a dominant seesaw pattern between anomalies in the midlatitudes and along the west coast of North America. In the surface layer (Fig. 12a1), there is a positive anomaly in the western and central midlatitudes, surrounded by a dominant negative anomaly along the North American coastal region and in the eastern and central subtropics. On the 25.2 kg m^{-3} isopycnal surface (Fig. 12b1), a positive tongue originates from the midlatitude outcrop region and extends southwestward around the subtropical gyre toward the western subtropics. This is accompanied by a negative anomaly located in the eastern coastal region. A similar spatial pattern can be seen on the 25.6 kg m^{-3} isopycnal surface but with the largest positive anomaly having become detached from the sea surface (Fig. 12c1). Farther down on the 26.0 kg m^{-3} isopycnal surface (Fig. 12d1), there is a large positive-anomaly band that extends from high latitude at 60°N, 170°E southeastward to about 40°N, 160°W. Compared with those in the shallower layers (Figs. 12b1,c1), there are pronounced negative anomalies in the subtropics that extend westward from the eastern boundary. The vertical structure of the first combined EOF mode along 157.5°W (Fig. 11b) shows a dominant positive-anomaly band that vertically penetrates downward and southward into the thermocline from the midlatitude outcrop region, accompanied by a negative anomaly in the subtropics.

The second combined EOF mode (the right panels in Fig. 12) clearly illustrates phase differences between temperature variability in the surface layer and in the thermocline, which are most evident in the eastern subtropics and Tropics. The temperature in the surface layer (Fig. 12a2) has a positive anomaly in the central midlatitudes, accompanied by a negative anomaly in the eastern subtropics and Tropics and by another small negative anomaly in the western subtropics at (40°N, 160°E). In the thermocline (Figs. 12b2–d2), on the other hand, there is a dominant positive anomaly in much of the basin, with the largest amplitude located in the western subtropics and Tropics, accompanied by a negative anomaly in the western subtropics and along the Kuroshio and its extension regions. In particular, there is an east–west-oriented negative anomaly band in the midlatitudes on the 26.0 kg m^{-3} isopycnal surface (Fig. 12d2). Figure 11c further shows the vertical structure of the second EOF mode along 157.5°W. Anomalies appear to be detached from the surface layer; a large positive anomaly is located around 23°N at the subsurface depth, accompanied by a negative anomaly in the midlatitudes (about 45°N) at depth and in the Tropics at the sea surface, respectively.

The EOF analysis above provides further evidence for the two preferred pathways around the North Pacific subtropical gyre. The two large-variability centers of the first EOF mode, which are out of phase, reflect the source regions of the two pathways (left panels in Fig. 12), one located in the eastern subtropics–Tropics and boundary regions, and the other centered in the midlatitude outcrop region. Since the first two leading combined EOF modes indicate a consistent phase relationship to one another, approximately in quadrature with EOF 1 leading EOF 2 by several years (Fig. 11a), a phase propagation phenomenon is suggested. These two leading modes, therefore, can be used to depict a dominant pattern of decadal thermocline variability around

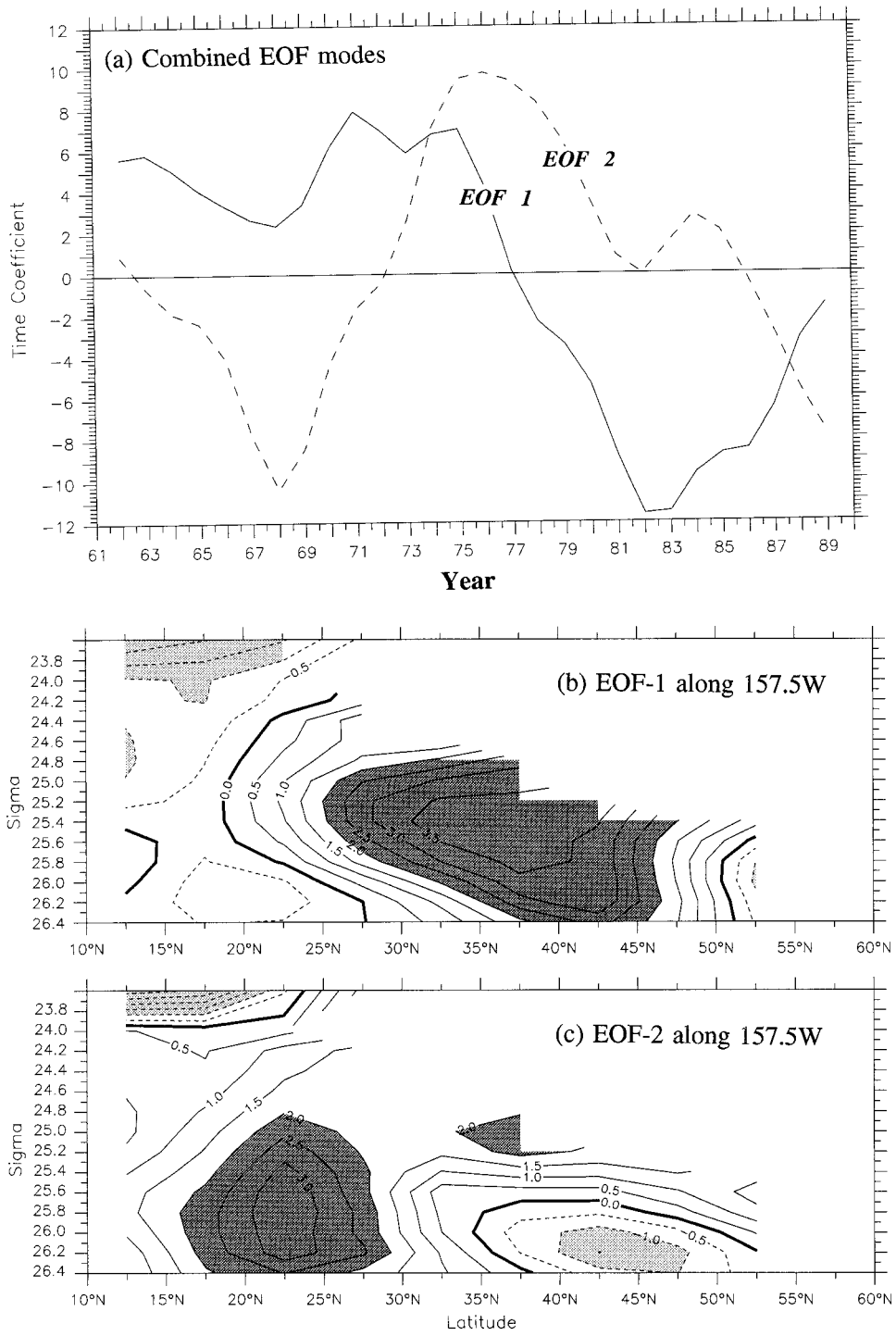

FIG. 11. Time variations and vertical structure of the first two combined EOF modes for temperature anomalies in the upper North Pacific Ocean. (a) The solid line for the first mode and the dashed line for the second mode; (b) the first eigenvector along 157.5°W; (c) the second eigenvector along 157.5°W. Contours in the eigenvector figures show the actual value multiplied by 100. The contour interval is 0.5 with the dashed line for negative areas.

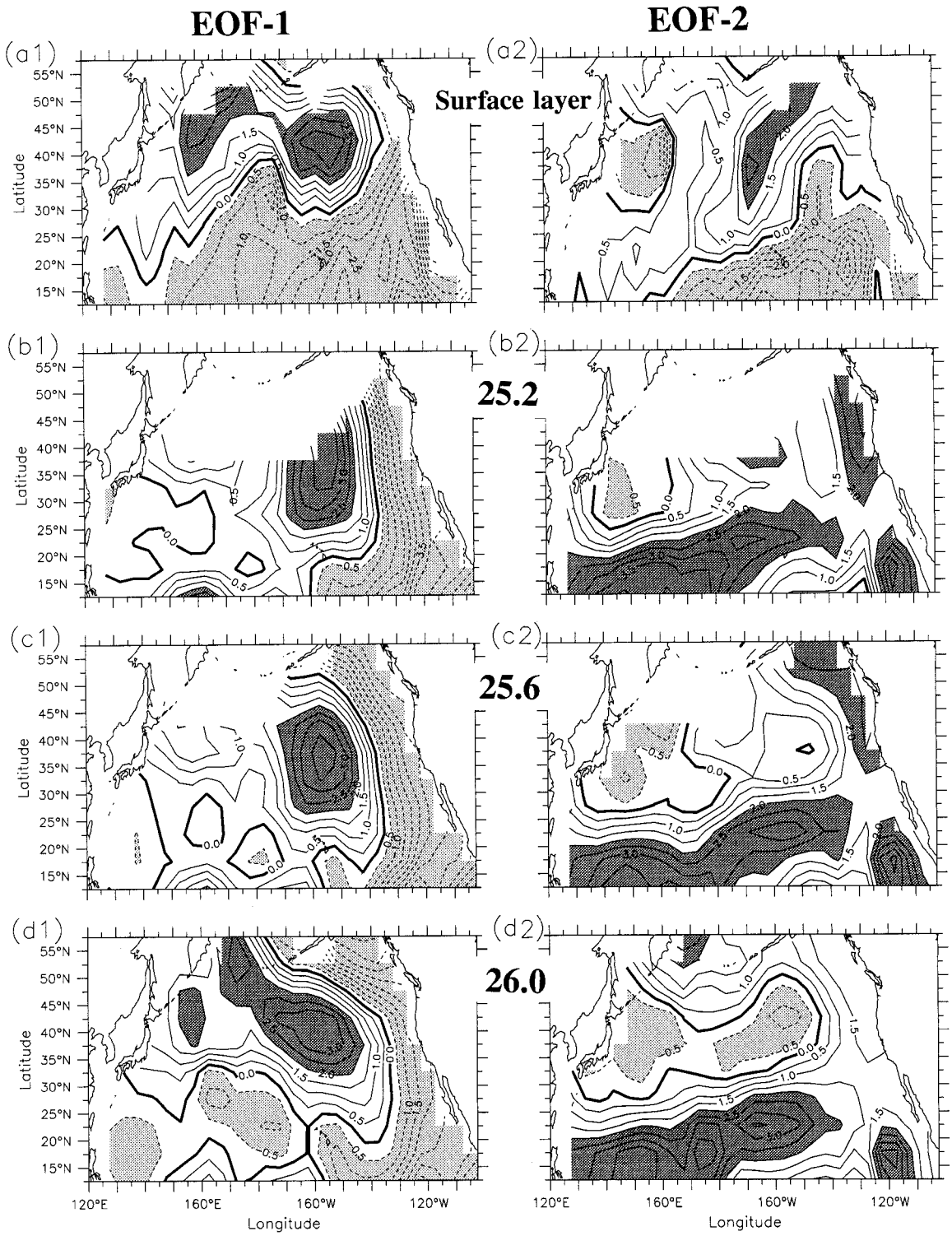

FIG. 12. Spatial patterns of the first (left panels) and second (right panels) combined EOF modes for temperature anomalies in the (a) surface layer, and on the (b) 25.2, (c) 25.6, and (d) 26.0 kg m^{-3} isopycnal surfaces. The contour information is the same as in Fig. 11.

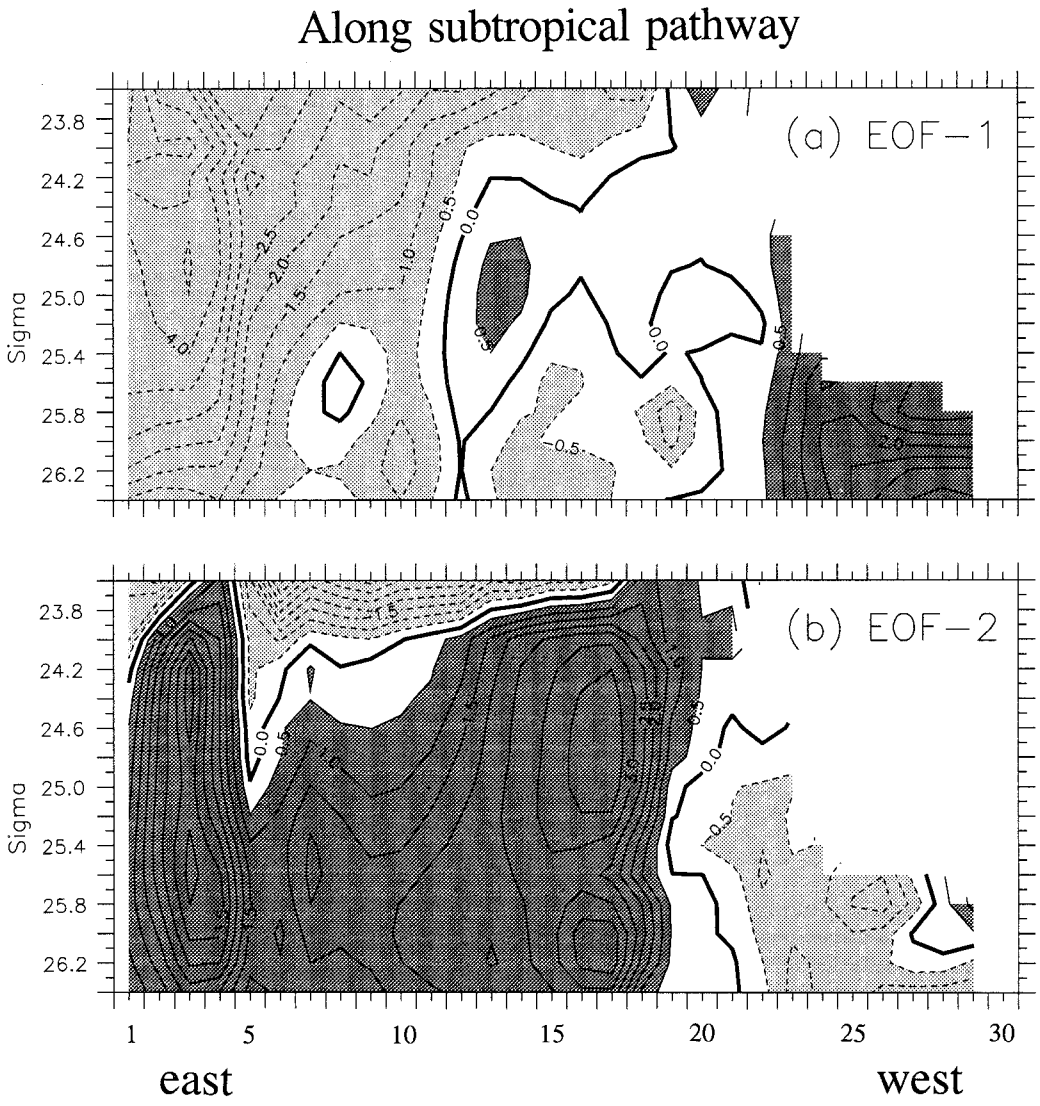

FIG. 13. The eigenvectors of the (a) first and (b) second combined EOF modes as a function of isopycnal surface and distance along the subtropical pathway (Fig. 2b). The horizontal axis gives numbers along the path from the start point near the eastern tropical boundary to the western midlatitudes through the subtropics.

the subtropical gyre: the spatial pattern described by the first EOF mode (Fig. 11b and the left panels in Fig. 12) will appear first, followed by that described by the second EOF mode (Fig. 11c and the right panels in Fig. 12). Consequently, a clear evolutionary picture can be demonstrated by sequentially tracing anomalies of the first EOF mode and of the second mode, respectively. Along the subduction pathway, the space–time evolution can be clearly seen in Figs. 11b,c for two combined EOF modes along 157.5°W. In Fig. 11b, we see a large positive anomaly in the midlatitude outcrop region, extending downward and southward from the sea surface. Several years later, as depicted by the second mode (Fig. 11c), the positive anomaly has moved to the subtropics–Tropics at depth, becoming detached from the sea surface. Along the subtropical pathway, the vertical structure of the two EOF modes is further shown in Fig. 13. The first mode shows a large negative anomaly in the eastern subtropics–Tropics and boundary regions (Fig. 13a). After several years, the negative anomaly, having propagated westward across the southern part of the subtropical gyre in the latitudinal band of 15°–30°N and farther along the Kuroshio path, is located in the western midlatitudes (Fig. 13b).

6. Summary and discussion

In this study, we document upper-ocean thermocline variability in the North Pacific on isopycnal surfaces over a 30-yr period from 1961 to 1990. EOF analyses have been performed on individual temperature anomaly fields on each single isopycnal as well as simulta-

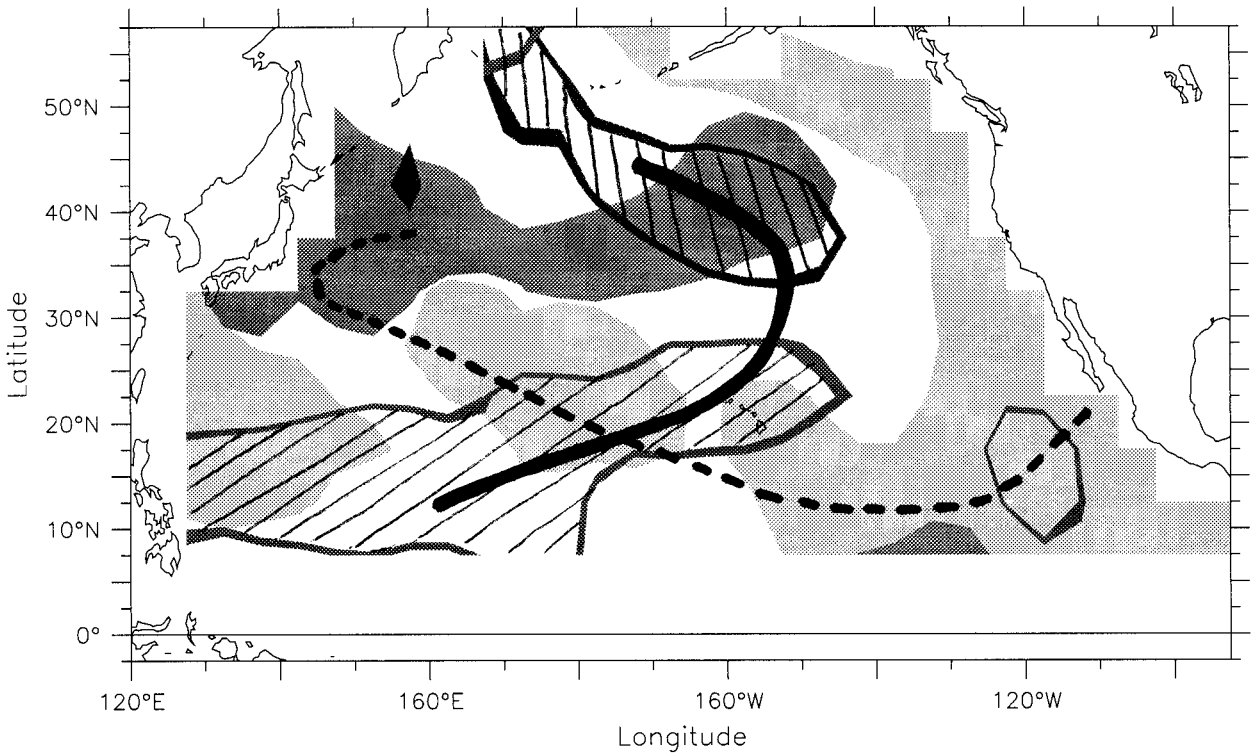

FIG. 14. A schematic diagram illustrating the two preferential pathways around the subtropical gyre associated with decadal thermocline variability in the North Pacific Ocean: a southwestward subduction pathway (solid line) and a westward subtropical pathway (dashed line). Superimposed are the eigenvector values of the first and second combined EOF modes on the 26.0 kg m^{-3} isopycnal surface replotted from Figs. 12d1 and 12d2. For clarity, only some eigenvector contours are shown: the lightly and heavily shaded regions indicate negative anomalies of the first (Fig. 12d1) and second (Fig. 12d2) EOF modes, respectively; the shaded lines with forward and backward diagonals pick out positive anomaly regions of the first (Fig. 12d1) and second (Fig. 12d2) EOF modes, respectively.

neously on all the upper-ocean data to depict the dominant three-dimensional patterns in a coherent way. Decadal thermocline anomalies appear to be well organized and tend to be more revealing on isopycnal surfaces; their basinwide evolution and transition signatures can be consistently traced in the thermocline around the subtropical gyre but not in the surface layer. The analysis has detected preferential thermocline variability patterns in the North Pacific, characterized by two dominant pathways around the subtropical gyre.

Figure 14 presents a schematic diagram of thermocline variability patterns around the North Pacific subtropical gyre, as represented by the combined EOF analysis (Figs. 11–13). Note that the two combined EOF modes show coherent phase relationships to one another, with the first leading the second by several years (Fig. 11a). We, therefore, first observe a pattern described by the first EOF mode: a positive anomaly band in the mid- and high latitudes, and a negative anomaly in the subtropics and along the west coast of North America. After several years, we then see a pattern described by the second mode: a positive anomaly located in the central and western Tropics, and a negative anomaly located in the western midlatitudes. Thus, the basinwide evolution features two preferential pathways around the subtropical gyre on decadal timescales: a dominant subduction pathway (the solid line in Fig. 14) and a subtropical pathway (the dashed line in Fig. 14). Along the former, surface temperature anomalies can be transferred downward into the thermocline in the midlatitude outcrop region (e.g., Fig. 11b). The subducted anomalies then move southward and westward around the subtropical gyre through the central–western subtropics into the Tropics (e.g., Fig. 11c). The latter extends from the eastern subtropics–Tropics and coastal regions and appears to continue predominantly westward in the subtropics and then northward and eastward along the Kuroshio path toward the midlatitudes (e.g., Fig. 13). Two examples of each type of anomaly pattern have been illustrated for the periods analyzed.

Since thermocline anomalies tend to be persistent and propagate around the gyre basin, they can have remote effects on SST and currents in other regions (e.g., Hirst and Godfrey 1993). Coherent basinwide propagation of thermocline anomalies along the two pathways may have remote effects around the subtropical gyre on decadal timescales. As demonstrated by Latif and Barnett (1994) and Jacobs et al. (1994), a propagating thermocline anomaly along the subtropical pathway may influence the strength of the Kuroshio and consequently

may contribute to surface-temperature changes along the Kuroshio and its extension regions, which may further induce variations in the atmosphere. This could trigger an unstable coupling between the atmosphere and ocean in the midlatitudes (e.g., Namias 1959; White and Barnett 1972; Latif and Barnett 1994, 1996; Jin 1997). As a result, air–sea interactions can be in operation and may produce large, persistent surface-temperature anomalies in the midlatitudes, which are subducted into the thermocline in the outcrop region; this provides a source from which the anomalies move on isopycnals along the subduction pathway toward the western subtropics and Tropics (Gu and Philander 1997; Zhang et al. 1998). It is also likely that the subducted anomaly may propagate into the Tropics with a wave motion (e.g., Lysne et al. 1997), instigated locally by decadal variations in wind stress curl patterns (e.g., Deser et al. 1999; Schneider et al. 1999). This may influence the thermal structure of the tropical Pacific Ocean, which, in turn, can feed back to the midlatitudes through the atmosphere (e.g., Graham 1994; Trenberth and Hurrel 1994) or through the ocean along the subtropical pathway. Thus, the subduction pathway indicates a connection of surface water-mass anomalies in the midlatitude outcrop regions to thermocline variations in the western subtropics and Tropics; the subtropical pathway may suggest a possible link of thermocline anomalies in the eastern Tropics–subtropics to surface temperature variations around the Kuroshio and its extension region, which may further force variations in the overlying atmospheric circulation in the midlatitudes. It is interesting to note that the two pathways proposed in this study constitute one important element of the two recently developed mechanisms for the Pacific decadal–interdecadal climate variability by Latif and Barnett (1994) and by Gu and Philander (1997), respectively.

The two pathways identified in our analysis seem to be consistent with recent development of ocean thermocline dynamics (e.g., Luyten et al. 1983; Liu 1993, 1996; Liu and Pedlosky 1994; Huang and Pedlosky 1999). Westward propagation has been observed by many previous studies both in thermocline temperature and in sea level. Theoretically, it can be related to planetary waves. As investigated by Liu (1999a,b), this signal resembles the first mode of baroclinic Rossby waves and has the strongest signals at the sea surface and at the bottom of the thermocline. This may explain why the subtropical pathway is observed most clearly on the shallow layers and in the low portions of the thermocline in our data analysis. This pattern may be generated most effectively by Ekman pumping (Liu 1999b). On the other hand, subduction is a well-known mechanism for thermocline variability (e.g., Luyten et al. 1983; Liu and Pedlosky 1994). A subduction path is basically determined by thermocline flow; the subducted temperature anomaly then tends to propagate with the subtropical gyre circulation. This subduction pattern can also be understood in terms of the second mode of planetary waves in the thermocline (Liu 1999a,b). This mode is strongly advected by mean flow and has a clear signature in the upper thermocline. This may explain why the subduction pathway is most salient in the upper thermocline in our data analysis. The thermocline variability pattern along the subduction pathway appears to be mainly forced by surface buoyancy anomaly in the midlatitude outcrop region (Liu and Pedlosky 1994; Liu 1999a,b; Huang and Pedlosky 1999; Schneider et al. 1999).

Our physical understanding of decadal thermocline variability in the Pacific is still in the early stages. The observed patterns and their time evolution are far from simple or obvious (Huang and Pedlosky 1999). It appears that a variety of mechanisms are present that may generate and maintain thermocline variability in the subtropics and in the midlatitudes, including remote processes (e.g., mean advection around the subtropical gyre and Rossby wave motion) and local processes (e.g., directly forced signals by wind changes). Based on very limited thermal data alone in this study, we are unable to provide a quantitative calculation to separate specific mechanisms responsible for the observed thermocline variability in different regions and the causal connection to SST anomalies. Also, the 30-yr observational record is obviously not long enough to establish the statistical significance of decadal variations. Since we have two realizations for each type of anomaly pathway during the analyzed periods, the results should be considered a case study. Clearly, the interpretation of data through model experiments and theoretical analyses are necessary. Much work is needed to improve our understanding of decadal–interdecadal climate change in the Pacific ocean–atmosphere system.

Acknowledgments. We are deeply indebted to S. Levitus and other staff at the Ocean Climate Laboratory (NOAA/NODC) for their help and support in analyzing observational data and for their unpublished materials. The historical oceanographic data used in this work are from the *NOAA Atlas NESDIS 5* (Levitus et al. 1994b). We would like to thank L. Rothstein, R. X. Huang, A. Busalacchi, S. Levitus, M. Latif, S. Tett, C. Deser, R. Lukas, J. Carton, and A. Miller for their helpful comments. We wish to thank two anonymous reviewers for their various comments and suggestions that helped to improve our original manuscript significantly. The editorial help of Ms. M. Kennedy is greatly appreciated. This research was supported by the NOAA Climate and Global Change Program (RHZ) and by the Physical Oceanography Program of NSF and the Young Investigator Program of ONR (ZL).

APPENDIX

The EOF Analysis

The EOF analysis has been extensively used to extract dominant time variations and spatial patterns of com-

plicated four-dimensional data (e.g., see North et al. 1982). We only briefly describe the essence of the method here. For a given anomaly field defined by

$$X(t) = [Xi(t)], \qquad i = 1, \ldots, I,$$

where i is the space index and I the total number of space points, the eigenfunctions of the covariance matrix, $[Xi(t)]$, can be obtained by a solution to the corresponding eigenvalue equation.

For the combined EOF analysis, the $Xi(t)$ includes simultaneously all temperature anomaly data on 14 layers [i.e., $i = 1, 2, \ldots, I_1, 1, 2, \ldots, I_2, \ldots, 1, 2, \ldots, I_{14}$, where I_j ($j = 1, 2, \ldots, 14$) is the number of space points on a given isopycnal surface; the total number of space points in the calculation of the combined eigenvalue equation is the sum of $I_1, I_2, \ldots, I_{14}$, respectively]. In our combined EOF analysis (section 5b), the number of space points on each layer are 259 (surface layer), 130 ($\sigma = 23.8$ kg m^{-3}), 149 ($\sigma = 24.2$ kg m^{-3}), 161 ($\sigma = 24.4$ kg m^{-3}), 176 ($\sigma = 24.6$ kg m^{-3}), 188 ($\sigma = 24.8$ kg m^{-3}), 198 ($\sigma = 25.0$ kg m^{-3}), 209 ($\sigma = 25.2$ kg m^{-3}), 216 ($\sigma = 25.4$ kg m^{-3}), 233 ($\sigma = 25.6$ kg m^{-3}), 242 ($\sigma = 25.8$ kg m^{-3}), 252 ($\sigma = 26.0$ kg m^{-3}), 252 ($\sigma = 26.2$ kg m^{-3}), and 257 ($\sigma = 26.4$ kg m^{-3}), respectively, with a total number of 2922 in space.

REFERENCES

Chelton, D. B., and M. G. Schlax, 1996: Global observations of oceanic Rossby waves. *Science,* **272,** 234–238.

Cox, M. D., and K. Bryan, 1984: A numerical model of the ventilated thermocline. *J. Phys. Oceanogr.,* **14,** 674–687.

Deser, C., M. A. Alexander, and M. S. Timlin, 1996: Upper-ocean thermal variations in the North Pacific during 1970–1991. *J. Climate,* **9,** 1840–1855.

——, ——, and ——, 1999: Evidence for a wind-driven intensification of the Kuroshio Current extension from the 1970s to the 1980s. *J. Climate,* **12,** 1697–1706.

Graham, N. E., 1994: Decadal scale variability in the tropical and North Pacific during the 1970's and 1980's: Observations and model results. *Climate Dyn.,* **10,** 135–162.

Gu, D.-F., and S. G. H. Philander, 1997: Interdecadal climate fluctuations that depend on exchanges between the tropical and extratropics. *Science,* **275,** 805–807.

Hautala, S. L., and D. H. Roemmich, 1998: Subtropical mode water in the Northeast Pacific Basin. *J. Geophys. Res.,* **103** (C6), 13 055–13 066.

Hirst, A. C., and J. S. Godfrey, 1993: The role of Indonesian Throughflow in a global ocean GCM. *J. Phys. Oceanogr.,* **23,** 1057–1086.

Huang, R. X., and S. Russell, 1994: Ventilation of the subtropical North Pacific. *J. Phys. Oceanogr.,* **24,** 2589–2605.

——, and J. Pedlosky, 1999: Climate variability inferred from a layered model of the ventilated thermocline. *J. Phys. Oceanogr.,* **29,** 779–790.

Jacobs, G. A., H. E. Hurlburt, J. C. Kindle, E. J. Metzger, J. L. Mitchell, W. J. Teague, and A. J. Wallcraft, 1994: Decade-scale trans-Pacific propagation and warming effects of an El Nino anomaly. *Nature,* **370,** 360–363.

Jin, F.-F., 1997: A theory of interdecadal climate variability of the North Pacific atmosphere–ocean system. *J. Climate,* **10,** 1821–1835.

Latif, M., and T. P. Barnett, 1994: Causes of decadal climate variability over the North Pacific and North America. *Science,* **266,** 634–637.

——, and ——, 1996: Decadal climate variability over the North Pacific and North America: Dynamics and predictability. *J. Climate,* **9,** 2407–2423.

Levitus, S., 1989: Interpentadal variability of temperature and salinity at intermediate depths of the North Atlantic Ocean, 1970–1974 versus 1955–1959. *J. Geophys. Res.,* **94,** 6091–6131.

——, and T. P. Boyer, 1994: *World Ocean Atlas 1994.* Vol. 4, *Temperature,* NOAA/NESDIS, 117 pp.

——, and J. Antonov, 1995: Observational evidence of interannual to decadal-scale variability of the subsurface temperature-salinity structure of the world ocean. *Climate Change,* **31,** 495–514.

——, R. Burgett, and T. P. Boyer, 1994a: *World Ocean Atlas 1994.* Vol. 3, *Salinity,* NOAA/NESDIS, 99 pp.

——, T. P. Boyer, and J. Antonov, 1994b: *World Ocean Atlas 1994.* Vol. 5, *Interannual Variability of Upper Ocean Thermal Structure,* NOAA/NESDIS, 176 pp.

Liu, Z., 1993: Thermocline forced by varying Ekman pumping. Part II: Annual and decadal Ekman pumping. *J. Phys. Oceanogr.,* **23,** 2523–2540.

——, 1996: Thermocline variability in different dynamic regions. *J. Phys. Oceanogr.,* **26,** 1633–1645.

——, 1999a: Planetary wave modes in the thermocline: Non-Doppler-shift mode, advective mode and Green mode. *Quart. J. Roy. Meteor. Soc.,* in press.

——, 1999b: Forced planetary wave response in a thermocline gyre. *J. Phys. Oceanogr.,* **29,** 1036–1055.

——, and J. Pedlosky, 1994: Thermocline forced by annual and decadal surface temperature variation. *J. Phys. Oceanogr.,* **24,** 587–608.

——, S. G. H. Philander, and R. C. Pacanowski, 1994: A GCM study of tropical–subtropical upper-ocean water exchange. *J. Phys. Oceanogr.,* **24,** 2606–2623.

Lozier, M. S., W. B. Owens, and R. G. Curry, 1995: The climatology of the North Atlantic. *Progress in Oceanography,* Vol. 36, Pergamon Press, 1–44.

Luyten, J. R., J. Pedlosky, and H. Stommel, 1983: The ventilated thermocline. *J. Phys. Oceanogr.,* **13,** 292–309.

Lysne, J., P. Chang, and B. Giese, 1997: Impact of the extratropical Pacific on equatorial variability. *Geophys. Res. Lett.,* **24,** 2589–2592.

McCreary, J. P., and P. Lu, 1994: Interaction between the subtropical and equatorial ocean circulations: The subtropical cell. *J. Phys. Oceanogr.,* **24,** 466–497.

Miller, A. J., D. R. Cayan, T. P. Barnett, N. E. Graham, and J. M. Oberhuber, 1994: The 1976–77 climate shift of the Pacific Ocean. *Oceanography,* **7,** 21–26.

——, ——, and W. B. White, 1998: A westward-intensified decadal change in the North Pacific thermocline and gyre-scale circulation. *J. Climate,* **11,** 3112–3127.

Namias, J., 1959: Recent seasonal interactions between North Pacific waters and the overlying atmospheric circulation. *J. Geophys. Res.,* **64,** 631–646.

North, G. R., T. L. Bell, R. F. Cahalan, and F. J. Moeng, 1982: Sampling errors in the estimation of empirical orthogonal functions. *Mon. Wea. Rev.,* **110,** 699–706.

Rothstein, L. M., R.-H. Zhang, A. J. Busalacchi, and D. Chen, 1998: A numerical simulation of the mean water pathways in the subtropical and tropical Pacific Ocean. *J. Phys. Oceanogr.,* **28,** 322–343.

Schneider, N., A. J. Miller, M. A. Alexander, and C. Deser, 1999: Subduction of decadal North Pacific temperature anomalies: Observations and dynamics. *J. Phys Oceanogr.,* **29,** 1056–1070.

Talley, L. D., 1988: Potential vorticity distribution in the North Pacific. *J. Phys. Oceanogr.,* **18,** 89–106.

Trenberth, K. E., and J. W. Hurrel, 1994: Decadal atmosphere–ocean variations in the Pacific. *Climate Dyn.,* **9,** 303–319.

White, W. B., and T. P. Barnett, 1972: A servomechanism in the ocean/atmosphere system of the mid-latitude North Pacific. *J. Phys. Oceanogr.,* **2,** 372–381.

——, and D. R. Cayan, 1998: Quasi-periodicity and global symmetries in interdecadal upper ocean temperature variability. *J. Geophys. Res.*, **103,** 21 335–21 354.

Zhang, R.-H., 1998: Decadal variability of temperature at a depth of 400 meters in the North Pacific Ocean. *Geophys. Res. Lett.*, **25,** 1197–1200.

——, and S. Levitus, 1997: Structure and cycle of decadal variability of upper-ocean temperature in the North Pacific. *J. Climate,* **10,** 710–727.

——, L. M. Rothstein, and A. J. Busalacchi, 1998: Origin of upper-ocean warming and El Niño change on decadal scale in the tropical Pacific Ocean. *Nature,* **391,** 879–883.